Chapter 2
FAULT IMPEDANCE LOOPS AND OVERHEAD LINE IMPEDANCE CALCULATIONS

2.1 Introduction

For the purpose of this study only the types of faults that occur more regularly on transmission power networks, such as single-phase-to-earth, phase-to-phase-to-earth and phase-to-phase faults will be discussed. The complete fault derivations are shown in Appendixes A, B, C and D. For consistency all symmetrical component calculations are shown using A-phase as reference. The intent of this section and that of section 2.2 is to refresh the reader's knowledge of the basic theory involved in system fault analysis. This theory is essential in understanding relay behaviour during power system faults. Sub-section 2.1.1 provides a summary of the symbols, suffixes and conventions used in this chapter and others to follow.

Section 2.3 will lead the reader through a detailed analysis of overhead line impedance calculations from first principles, whilst section 2.4 will provide some insight into the effect that different load configurations could have on relay measurements. Protection relays are set based on the parameters obtained from the power network, and as such it is imperative that all high voltage equipment parameters be obtained to the highest level of accuracy possible. Incorrect relay settings due to power system parameters could cause relay overreach to occur resulting in unnecessary operation and subsequent tripping (disconnection) of healthy primary equipment. The impact of incorrect protection relay settings will become more apparent in Chapter 5.

2.1.1 Symbols and conventions used

In this dissertation the symmetrical calculations are all shown with A-phase as reference, the suffix "a" in all symmetrical component equations has been neglected. The sequence components will simply be referred to as V_0, V_1, V_2 and I_0, I_1 and I_2 for the sequence voltages and currents respectively. Network sequence impedances will be identified as Z_0, Z_1 and Z_2, with phase impedances Z_a, Z_b and Z_c. The suffixes

"0", "1" and "2" refers to zero, positive and negative sequence. In all other equations the suffixes "a", "b" and "c" refer to phase A, B and C respectively, whilst as per normal reference the notation "V" refers to phase voltage and "I" to the phase current in an AC circuit. The suffix "F" will in all cases be used to identify a faulted phase voltage, current or fault impedance and resistance. The alpha (α) multiplier identifies a 120° phase shift between the relevant phase and sequence components.

2.1.2 Single-phase-to-earth fault loop

As has already been mentioned, single-phase-to-earth faults occur often on overhead transmission lines. It is therefore important that a thorough understanding of this type of fault under different system conditions is obtained. The relevance of this section and others pertaining to theoretical fault analysis will become clearer in the fault analysis and relay operation evaluation in Chapter 5 and Chapter 6. The theoretical equation derivation for an A-phase-to-earth fault is shown below. It is important to note that these derivations are made from a simplistic radial network with a single source of supply. A typical single-phase-to-earth fault in a radial network with source voltages E_a, E_b and E_c, line currents I_a, I_b and I_c, fault impedance Z_F and no-load connected is shown in Figure 2.1. Load configurations will be discussed in section 2.4, whilst the impact that load has on protection relay measurement will be analysed in Chapter 3, section 3.2.7 and section 3.3.8 and again later in Chapter 6, section 6.1.3. The impact of complex networks on relay measurement, with multiple sources connected at different locations in the power network, will be discussed in more detail in Chapter 4.

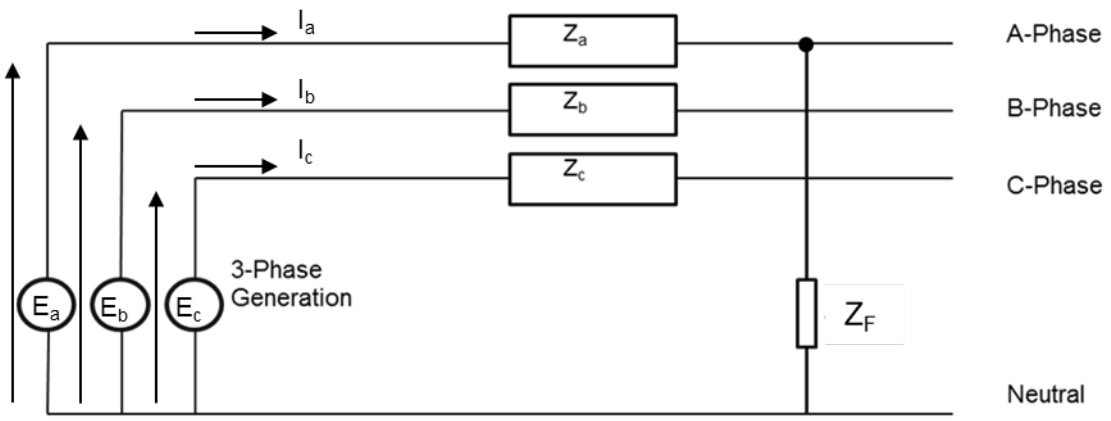

Figure 2.1: A-phase-to-earth fault

From Figure 2.1 the following conclusions can be made

At the point of fault for $Z_F = 0$ [5], [9], [12]

$$V_a = 0 \tag{2.1}$$

$$I_b = I_c = 0 \tag{2.2}$$

If fault impedance exists at the point of fault, the condition for V_a changes to

$$V_a = I_F Z_F \tag{2.3}$$

It should already be noted at this point that the assumption of $I_b = I_c$ is only valid for the simplified radial system with no load connected. With load connected I_b would not necessarily be equal to I_c,

Assigning I_b and I_c to its symmetrical components, then, through mathematical manipulation it can be shown that for $V_a = 0$

$$I_a = \frac{3E}{Z_1 + Z_2 + Z_0} \tag{2.4}$$

and for $V_a = I_F Z_F$

$$I_a = \frac{3E}{Z_1 + Z_2 + Z_0 + 3Z_F} \tag{2.5}$$

From Eq. (2.4) and Eq. (2.5) it is possible to derive the generic equation for the positive sequence impedance given in Eq. (2.6) and Eq. (2.7) respectively. For the complete derivation see Appendix A.

$$Z_1 = \frac{E}{\left(I_a + 3I_0K_0\right)} \tag{2.6}$$

and

$$Z_1 = \frac{E - 3I_0R_F}{\left(I_a + 3I_0K_0\right)} \tag{2.7}$$

where

$$K_0 = \frac{1}{3}\left(\frac{Z_0}{Z_1} - 1\right) \tag{2.8}$$

E = pre-fault or Thevenin's voltage at the point of fault just prior to the fault. Since the majority of system faults that occur on the Eskom transmission system are single-phase-to-earth faults, only the full sequence component analysis for these types of faults will be shown. A faulted circuit can theoretically be broken down into a combination of positive, negative and zero-sequence networks. The simplified diagram of Figure 2.2 depicts the theoretical network for a radial transmission network. The source voltage E and network sequence components of voltage (V_1, V_2, V_0), current (I_1, I_2, I_0) and impedances (Z_1, Z_2, Z_0) are shown. In this instance the assumption that the fault reactance X_F = 0 is made and therefore only the fault resistance R_F is shown.

It is important to note that the equivalent circuit for a complex transmission network is vastly different from a radial network. The exact nature of these differences will be discussed in more detail later in this dissertation.

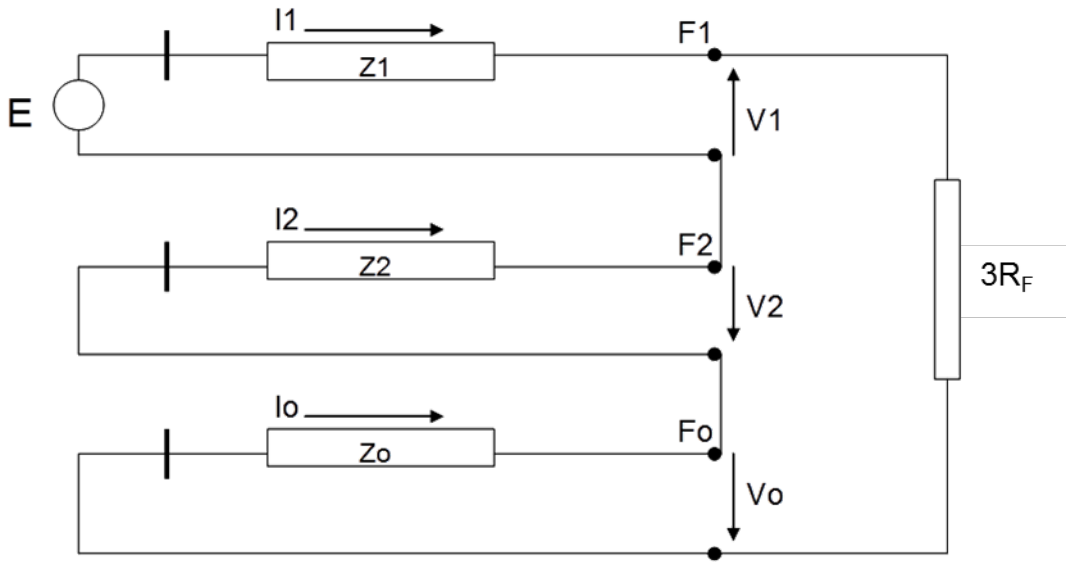

Figure 2.2: Phase-to-earth fault theoretical diagram

From Figure 2.2 the following is evident at the point of fault

$$V_1 = E - I_1 Z_1 \tag{2.9}$$

$$V_2 = 0 - I_2 Z_2 \tag{2.10}$$

$$V_0 = 0 - I_0 Z_0 \tag{2.11}$$

For this type of fault the following relationships for the faulted phase voltage is obtained

$$V_{a_F} = V_1 + V_2 + V_0 \tag{2.12}$$

$$V_{a_F} = E - I_1 Z_1 - I_2 Z_2 - I_0 Z_0 \tag{2.13}$$

$$I_a = I_1 + I_2 + I_0 \tag{2.14}$$

since

$$I_1 = I_2 = I_0 \tag{2.15}$$

therefore

$$I_a = 3I_1 \tag{2.16}$$

also the sequence impedance

$$Z_1 = Z_2 \tag{2.17}$$

Using Eq. (2.13) and Eq. (2.17) it now follows that

$$V_{a_F} = E - I_1(2Z_1 + Z_0) \tag{2.18}$$

also

$$V_{a_F} = 3I_1R_F \tag{2.19}$$

therefore

$$3I_1R_F = E - I_1(2Z_1 + Z_0) \tag{2.20}$$

hence

$$E = I_1(2Z_1 + Z_0) + 3I_1R_F \tag{2.21}$$

$$\frac{E}{3I_1} = \frac{1}{3}(2Z_1 + Z_0) + R_F \tag{2.22}$$

and

$$\frac{E}{I_a} = \frac{1}{3}(2Z_1 + Z_0) + R_F \tag{2.23}$$

In the simplified circuit the positive sequence source voltage E is also the phase voltage V_a at the relaying point. Assuming balanced conditions prior to the fault and from the voltage relationship given by Eq. (2.24) it follows that the loop impedance (V_a/I_a) measured by the relay is given by Eq. (2.25).

$$V_{a1} = \frac{1}{3}(V_a + \alpha \mathrm{V_b} + \alpha^2 \mathrm{V_c}) \tag{2.24}$$

$$Z_{loop} = \frac{V_a}{I_a} = \frac{1}{3}(2Z_1 + Z_0) + R_F \tag{2.25}$$

This is the exact equation as is used by the relay manufacturer for relay B in the determination of the single-phase-to-earth zone measuring element as shown in Chapter 3 section 3.3.

2.1.3 Phase-to-phase-to-earth fault loop

Phase-to-earth faults sometimes develop into phase-to-phase-to-earth faults. Protection relays needs to be sensitive to this change in fault and operate accordingly in order to clear the fault quickly and correctly and initiate the correct auto-reclose sequence. This phenomenon is discussed again in Chapter 5 during protection relay operation analysis. Figure 2.3 depicts a two phase-to-earth fault with possible fault impedances existing between phases and phase-to-earth. It will be used to identify the different voltage and current conditions applicable to this type of fault, from which the relevant fault equations can be developed.

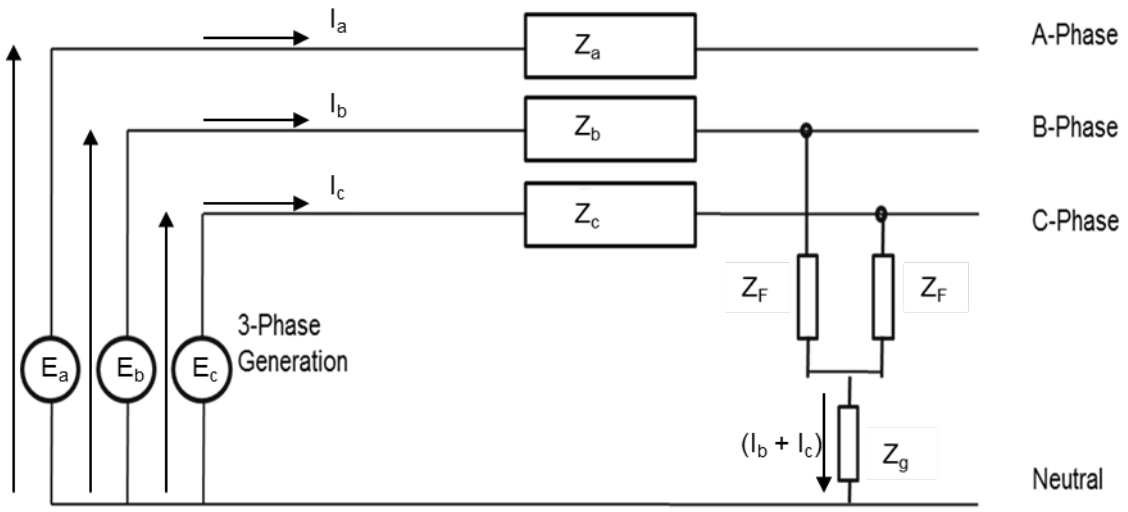

Figure 2.3: B-C Phase-to-earth fault

From Figure 2.3 the following conclusions can be made

At the point of fault with no fault resistance (Z_F & Z_g = 0) [5]

$$I_a = 0 \tag{2.26}$$

$$V_b = V_c = 0 \tag{2.27}$$

At the point of fault with fault resistance ($Z_g > 0$) [9]

$$V_b = V_c = Z_g(I_b + I_c) \tag{2.28}$$

At the point of fault with fault resistance between phases and to earth [12]

$$V_b = V_c = (Z_F + Z_g)I_b + \left(Z_F + Z_g\right)I_c \tag{2.29}$$

Note that for this scenario $I_a = 0$, but this may not be true with load connected to the circuit. After assigning V_b and V_c to its symmetrical components and through mathematical manipulation it can be shown that [5]

$$E = I_1\left[Z_1 + \frac{Z_2 Z_0}{Z_2 + Z_0}\right] \tag{2.30}$$

For a single A-phase-to-earth fault the phase currents are given by [5]

$$I_a = I_1 + I_2 + I_0 = 0 \tag{2.31}$$

$$I_b = \frac{-j\sqrt{3}E\left(Z_0 - \alpha Z_2\right)}{Z_1 Z_2 + Z_2 Z_0 + Z_0 Z_1} \tag{2.32}$$

$$I_c = \frac{j\sqrt{3}E\left(Z_0 - \alpha^2 Z_2\right)}{Z_1 Z_2 + Z_2 Z_0 + Z_0 Z_1} \tag{2.33}$$

For complete derivation see Appendix B.

For the cases where fault resistance exists between phases or between phases and earth, the phase currents can be obtained using sequence Eq. (2.34), Eq. (2.35) and Eq. (2.36) [9].

For the condition where fault resistance exists between phases the sequence currents are given by [9]

$$I_1 = \frac{V_F}{Z_1 + \left[\frac{Z_2(Z_0 + 3Z_F)}{Z_2 + Z_0 + 3Z_F}\right]} \tag{2.34}$$

$$I_2 = (-I_1)\left(\frac{Z_0 + 3Z_F}{Z_0 + 3Z_F + Z_2}\right) \tag{2.35}$$

$$I_0 = (-I_1)\left(\frac{Z_2}{Z_0 + 3Z_F + Z_2}\right) \tag{2.36}$$

When considering the condition of a phase-to-phase-to-earth fault with fault resistance between phases and to earth, the phase currents can be obtained using phase sequence Eq. (2.37) and Eq. (2.38) and Eq. (2.39) [12].

$$I_1 = \frac{V_F}{Z_1 + Z_2 + \frac{(Z_2 + Z_F)(Z_0 + Z_F + 3Z_g)}{Z_0 + Z_2 + 2Z_F + 3Z_g}} \tag{2.37}$$

$$I_2 = \frac{Z_0 + Z_F + 3Z_g}{Z_2 + Z_0 + 2Z_F + 3Z_g} \tag{2.38}$$

$$I_0 = \frac{Z_2 + Z_F}{Z_2 + Z_0 + 2Z_F + 3Z_g} I_1 \tag{2.39}$$

The phase currents for both cases can now be obtained using the well-known matrix

$$\begin{bmatrix} I_A \\ I_B \\ I_C \end{bmatrix} = \begin{bmatrix} 1 & 1 & 1 \\ 1 & a^2 & a \\ 1 & a & a^2 \end{bmatrix} \cdot \begin{bmatrix} I_0 \\ I_1 \\ I_2 \end{bmatrix} \tag{2.40}$$

From the phase voltages and currents the phase loop impedance can be calculated. For B-phase-to-earth, the loop impedance is given by [12]

$$Z_b = Z_{b-g} = \frac{V_{b-g}}{I_{b-g}} \tag{2.41}$$

From Figure 2.4 the following conclusions can be made

At the point of fault for $Z_F = 0$ [5]

$$I_a = 0 \tag{2.42}$$

$$I_b + I_c = 0 \tag{2.43}$$

$$V_b = V_c = V \tag{2.44}$$

2.1.4 Phase-to-phase fault loop

Phase-to-phase fault loops are similar to phase-to-phase-to-earth faults. Although less in occurrence, these types of faults do happen and needs to be catered for correctly. Protection relay operation in this case should be such as to trip the required feeder breaker three-pole. A typical relay operational scenario is discussed in Chapter 5, section 5.3. A phase-to-phase fault involving B and C-phase with fault impedance can be represented by the drawing shown in Figure 2.4. The relevant fault equations for a typical B-C-phase fault can be obtained using this figure as guide. For complete derivations see Appendix C.

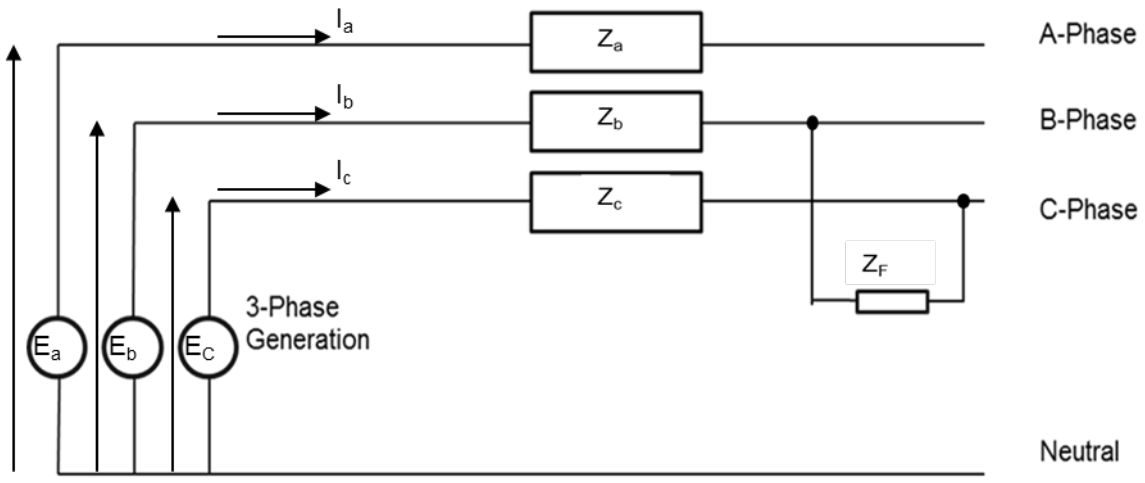

Figure 2.4: B-C-Phase fault

The following equations and assumptions can be made

Eq. (2.44) is no longer valid when $Z_F > 0$. For this scenario, we need to use Eq. (2.45) as given below [9], [12].

$$(V_b - V_c) = Z_F I_b \tag{2.45}$$

Note that $I_a = 0$ in this case may also be different with load connected.
Hence after assigning V_b, V_c, I_b and I_c to their respective symmetrical components and through mathematical manipulation it can be shown that [5]

$$E = I_1(Z_1 + Z_2) \tag{2.46}$$

$$I_a = I_1 + I_2 = 0 \tag{2.47}$$

$$I_b = \frac{-j\sqrt{3}E}{Z_1 + Z_2} \tag{2.48}$$

$$I_c = \frac{j\sqrt{3}E}{Z_1 + Z_2} \tag{2.49}$$

The following sequence equations are valid when $Z_F > 0$ [9], [12]

$$I_1 = \frac{V_F}{(Z_1 + Z_2 + Z_F)} \tag{2.50}$$

$$I_b = \frac{-j\sqrt{3} \cdot V_F}{(Z_1 + Z_2 + Z_F)} \tag{2.51}$$

$$I_c = \frac{j\sqrt{3} \cdot V_F}{(Z_1 + Z_2 + Z_F)} \tag{2.52}$$

2.2 Complex impedance calculations

For networks with multiple sources, where the point of interest has a source or sources behind and in front of the relaying point it is essential to calculate the equivalent source and impedance correctly in order to obtain the correct fault current at the point of fault and at the relaying location. Multiple source networks also complicates post mortem fault analysis in that protection relays can only operate based on the quantities that it measures. Various factors such as fault resistance, earth-wire continuity and in-feed from sources located in front of the relaying position, etc. can influence the quantities measured by a protection relay. For these reasons different network theorems have been developed to simplify complicated interconnected networks. Reducing the network sources, of any linear network, to a representative equivalent source is important especially when different source voltages are present in the network, which is often the case [5].

Although there are several network theorems, only some of the relevant theorems applicable to linear networks will be shown in the following sub-sections. Application of these theorems in actual complex system fault calculations are explored in Chapter 4, section 4.3, these theories were also used in the development of Matlab based routines used in the relay algorithm comparisons discussed in Chapter 4.

2.2.1 Parallel connected sources and branch/equipment impedances

In effectively earthed multiple source networks, these sources are invariably connected in parallel. It is therefore essential to understand how these multiple source networks can be simplified into a single source of supply. Calculation of total fault current of any type of fault, at any point of a complex multiple source network, is made possible. Accurate calculation of fault levels in any part of a network is necessary in order to specify new high voltage equipment ratings as well as setting protection relay measuring elements. In a parallel connected network, illustrated by Figure 2.5, the effective voltage source (E_r) and branch/equipment impedance is obtained through the use of Eq. (2.53) and Eq. (2.54) given below [5]. The different

source voltages in the network shown is given by E_1, E_2 and E_3, with the different network admittances being represented by Y_1, Y_2 and Y_3. The resultant parallel source voltage (E_r) and network admittance (Y_r)as depicted in Figure 2.5 is given by

$$E_r = \left(1 \middle/ Y_r \right) \sum_i E_i Y_i \tag{2.53}$$

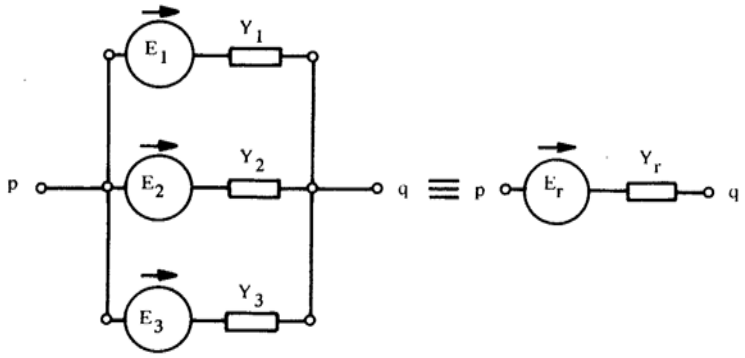

Figure 2.5: Parallel source and admittance branches [5]

where

$$Y_r = \sum_i Y_i \tag{2.54}$$

From Eq. (2.53) and Eq. (2.54) above it is evident that the resultant voltage source (E_r) is obtained from the vector sum of the parallel source voltages multiplied with its own relative series admittance and multiplied by the inverse resultant admittance.

2.2.2 Equal source voltages

In a complex network with multiple equal source voltages connected to a common node, the situation is rather simple and all sources can be replaced by a single source voltage of equal magnitude and angular relationship connected to the common node. This theorem therefore allows the connection of different busbars together within the same network that are at the same voltage potential [5]. Figure 2.6 illustrates this theorem graphically. The resultant source voltage is then given by

$$E_r = E_1 = E_2 \tag{2.55}$$

The downfall of the implementation of this method in practice is that inevitably different sources exists in a power system and unless connected to the same busbar is not equal in magnitude and angle.

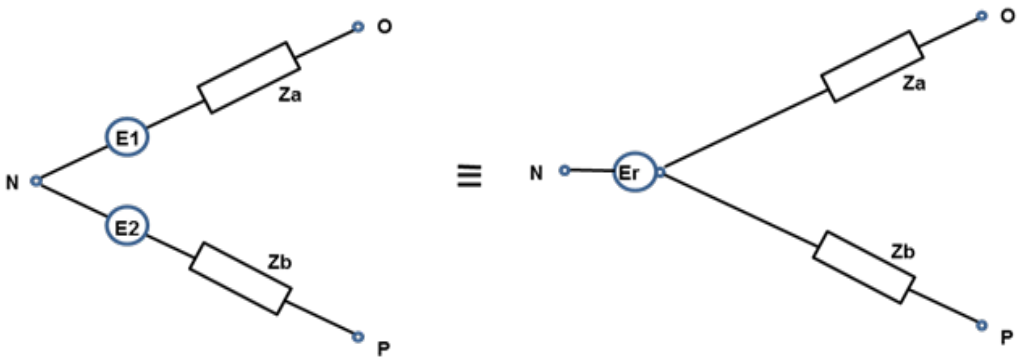

Figure 2.6: Reduction of equal source voltages [5]

2.2.3 Superposition method

With the method of superpositioning, illustrated in Figure 2.7, the fault currents that flow in any branch as a result of several source voltages can be obtained. The total branch current is obtained by the vector sum of the currents in each branch. These branch currents are obtained through individual application of the different source voltages with all the other source voltages short circuited [5].

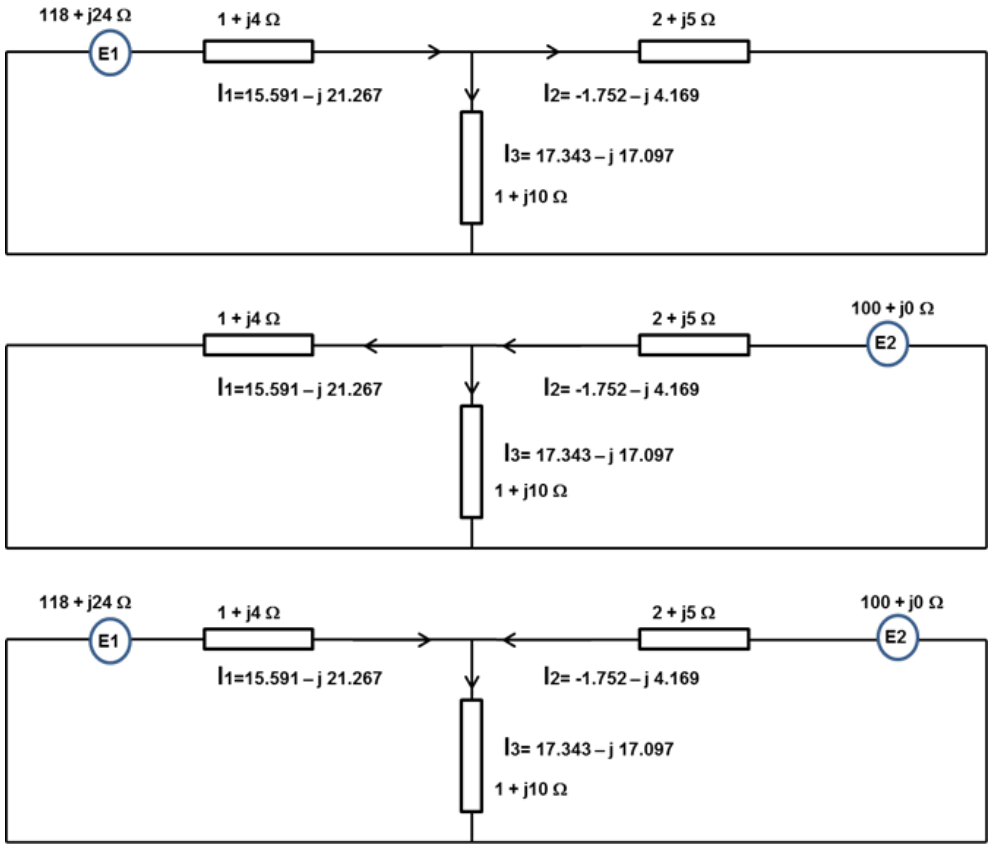

Figure 2.7: Graphical superposition illustration [5]

2.2.4 Thevenin's theory

Thevenin's theory states that any linear network viewed from any two terminals within the network can be replaced by a single source voltage in series with network equivalent impedance. The Thevenin voltage is represented by the open-circuit voltage between the relevant terminals. This open-circuit voltage is equal to the resultant parallel source voltage (E_r) determined by Eq. (2.53) for no-load conditions [5].

The pre-fault voltage (V_{pF}) indicated in Figure 2.8 represents the Thevenin open-circuit voltage at bus B. In Figure 2.8 the network source impedances are represented by Zs1and Zs2, the transformer impedances by Z_T A and Z_T B, loads by ZLoad 1 and ZLoad 2, with the line impedances between busbars A and B and busbars B and C as Z_L AB and Z_L BC respectively. The parallel source method described in section 2.2.1 can therefore be used to calculate the total fault current where the actual source voltages at the instant just prior to fault inception are known.

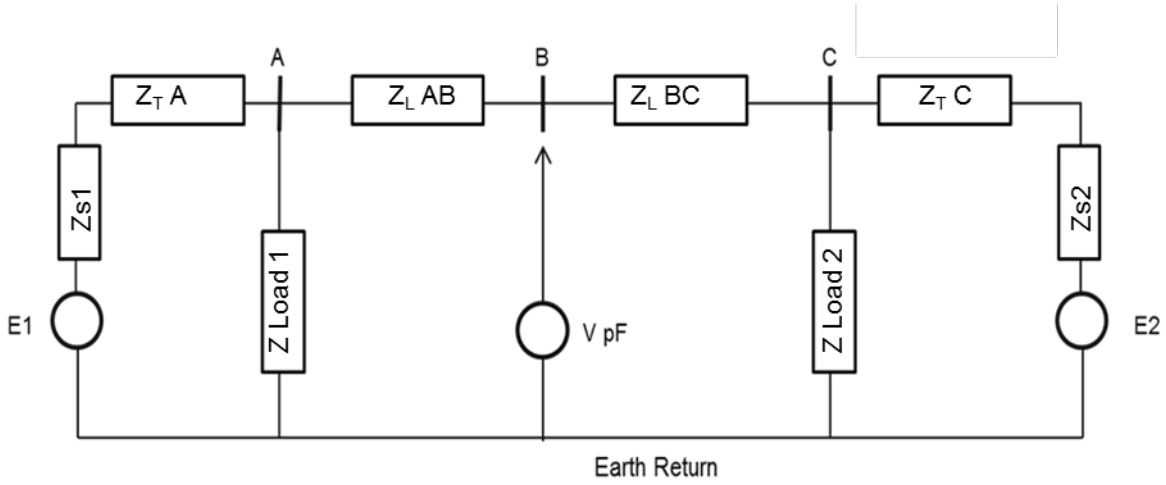

Figure 2.8: Thevenin open-circuit pre-fault voltage illustration

The same is true for the super positioning method discussed in section **Error! Reference source not found.**. The Thevenin method determines the pre-fault voltage at the point of fault, prior to the fault. The pre-fault voltage at the point of fault is a function of the load current circulating through the part of the network of interest and the source voltages. In general the Thevenin method is preferred due to the fact that for most system faults the pre-fault voltages and load currents are available from recording devices at stations close to the actual fault. From these recordings fairly accurate pre-fault voltages can be determined at the point of fault, provided that the point of fault is known. A combination of the pre-fault and super positioning methods is then used to determine the actual fault currents and the total currents in any of the branches in the network. This concept will be discussed in more detail in Chapter 4.

In order to simplify initial conditions it is often assumed that the source voltages are equal in size and magnitude during no-load conditions. In strong power systems

with small source impedances the ratio between fault current and load current is rather large and therefore the impact of load current on protection relay measurement is small. This is true since the load impedance, which is a function of the connected load in MVA and the applied load voltage, is large when compared to high voltage equipment impedances connected in series with the load [5].

This is not the case in weaker systems where load currents become comparable with fault currents. This phenomenon is easily demonstrated with the use of a simple system as shown in Figure 2.9 to Figure 2.12. Figure 2.9 and Figure 2.11 represents the busbar voltage in kV and phase angle, whilst for the feeders and transformers the load currents in kA and phase angles are indicated for the load-flow solution. Fault currents in kA and phase angles for three-phase fault conditions are shown in Figure 2.10 and Figure 2.12.

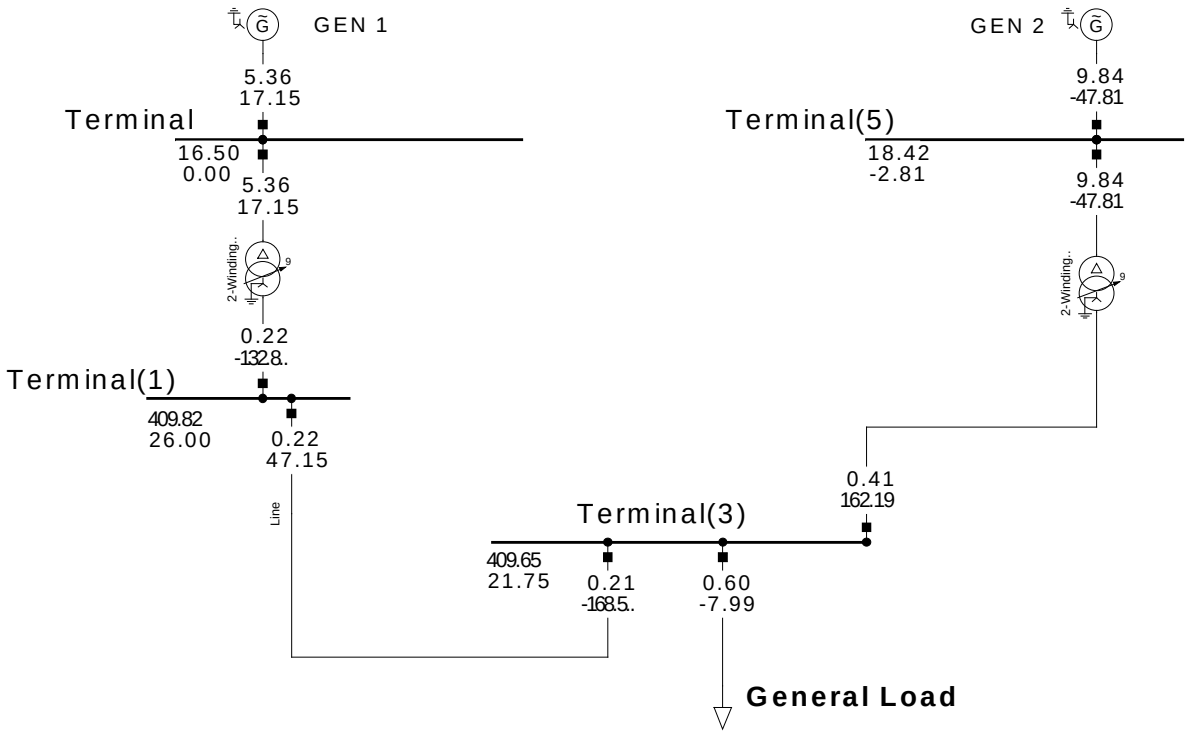

Figure 2.9: Load-flow with strong source

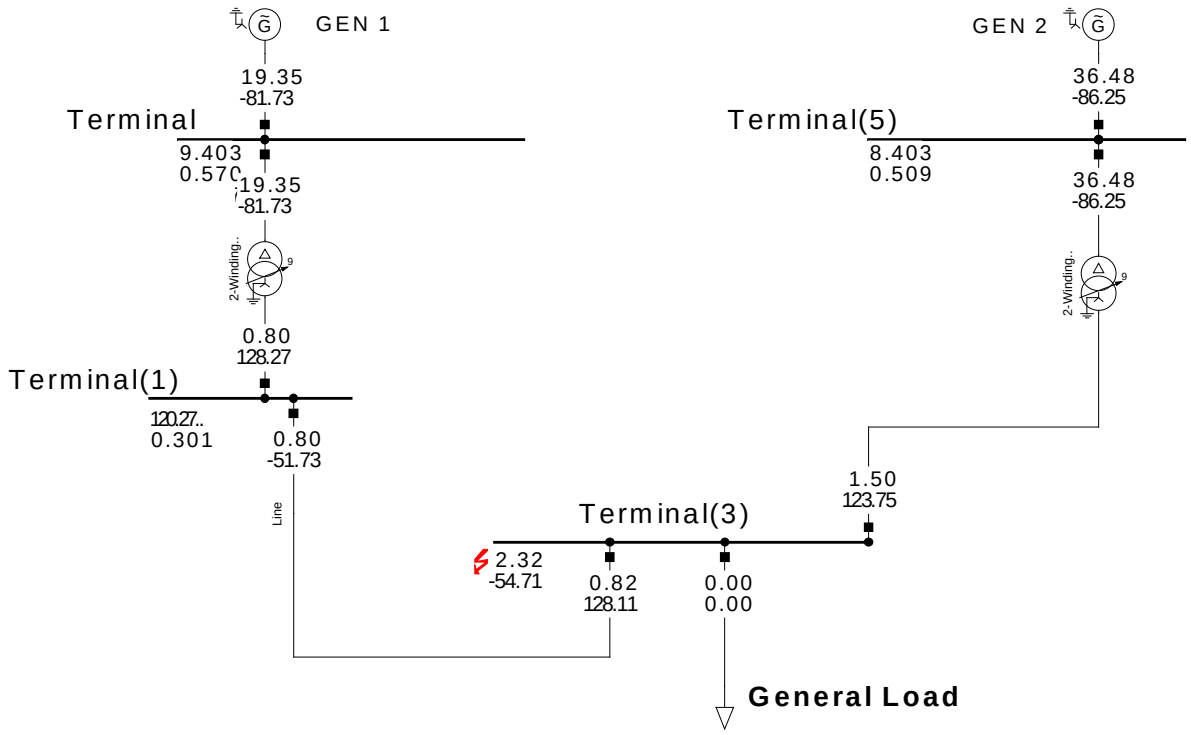

Figure 2.10: Three-phase fault with strong source

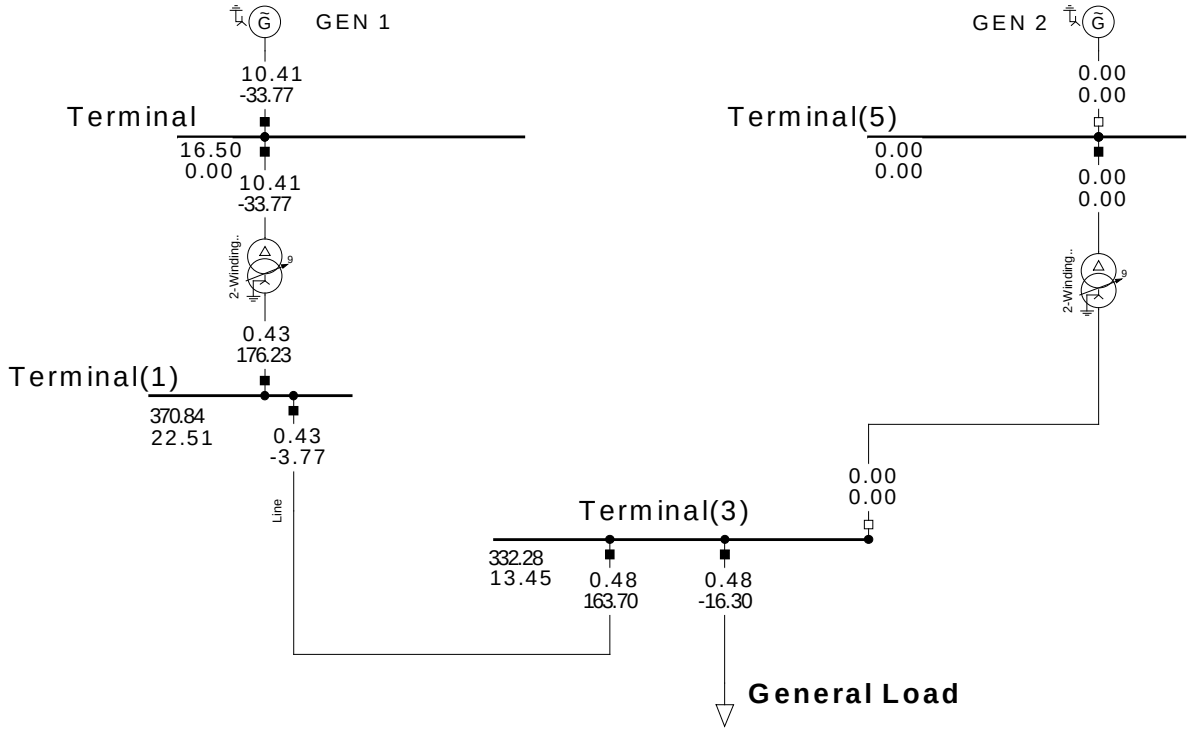

Figure 2.11: Load-flow with weak (single) source

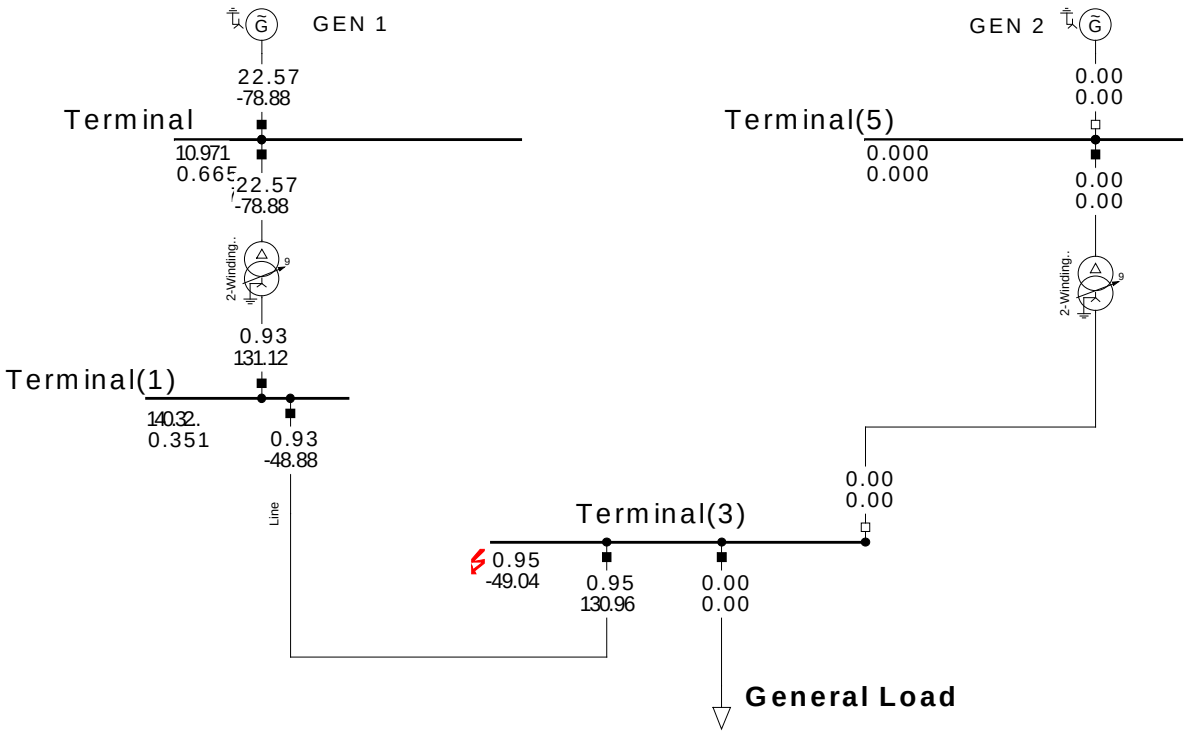

Figure 2.12: Three-phase fault with weak source

The following information can easily be obtained from these figures

Strong Source Condition

- No significant drop in voltage at the different 400 kV terminals during normal load-flow conditions.
- The General Load consumes a total of 600 A (see Figure 2.9).
- Three-phase fault current for a fault at Terminal (3) is a maximum at 2.32 kA. (see Figure 2.10).

Weak Source Condition

- The busbar voltage at 400 kV Terminal (1) drops to 370.84 kV during normal load-flow conditions (see Figure 2.11).
- The load current drops to 480 A with the same connected load.
- Three-phase fault current at Terminal (3) drops from 2.32 kA to only 950 A (see Figure 2.12).

It is clear therefore that for a specific load, the applied voltage dictates the load current. Eq. (2.56) to Eq. (2.59) can be used to calculate per unit impedance of the

load based on the applied voltage and selected load when the voltage applied is known [5].

$$I_b = S_b / \sqrt{3} * V_b \tag{2.56}$$

$$V_{L(pu)} = V_{app} / V_{net} \tag{2.57}$$

$$I_{L(pu)} = I_{L(app)} / I_b \tag{2.58}$$

$$Z_{L(pu)} = V_{L(pu)} / I_{L(pu)} \tag{2.59}$$

where

I_b = the base current.

S_b = MVA base

V_b = Voltage base in kV

V_{app} = voltage applied to the load

$V_{L(pu)}$ = load voltage in per unit of applied voltage

$I_{L(app)}$ = load current due to voltage applied

$I_{L(pu)}$ = load current in per unit

Transformer star-point and/or load earthing has no impact on balanced three-phase system faults [5]. It does however play a major role in the distribution of unbalanced fault currents involving earth return. The positioning and number of earthed transformer star-points in relationship with the position of fault will therefore determine the magnitude of unbalanced fault current and the distribution of such fault currents through the network. This statement is better understood with the use of a small network (see Figure 2.13).

For an A-phase-to-earth fault on Line 1 with no fault resistance, twenty percent of the line length from Terminal 9, the zero-sequence current contribution is 870 A and 1.13 kA respectively. The strongest zero sequence contribution come from Terminal 6, which has the majority of earthing points, supplied by the three earthed transformers. Most importantly is the fact that although the fault is closest to Terminal 9, the fault current contribution from this side is much less than that from Terminal 6. Protection

relays therefore need to be set carefully at Terminal 6 in order to detect single-phase faults further down the line.

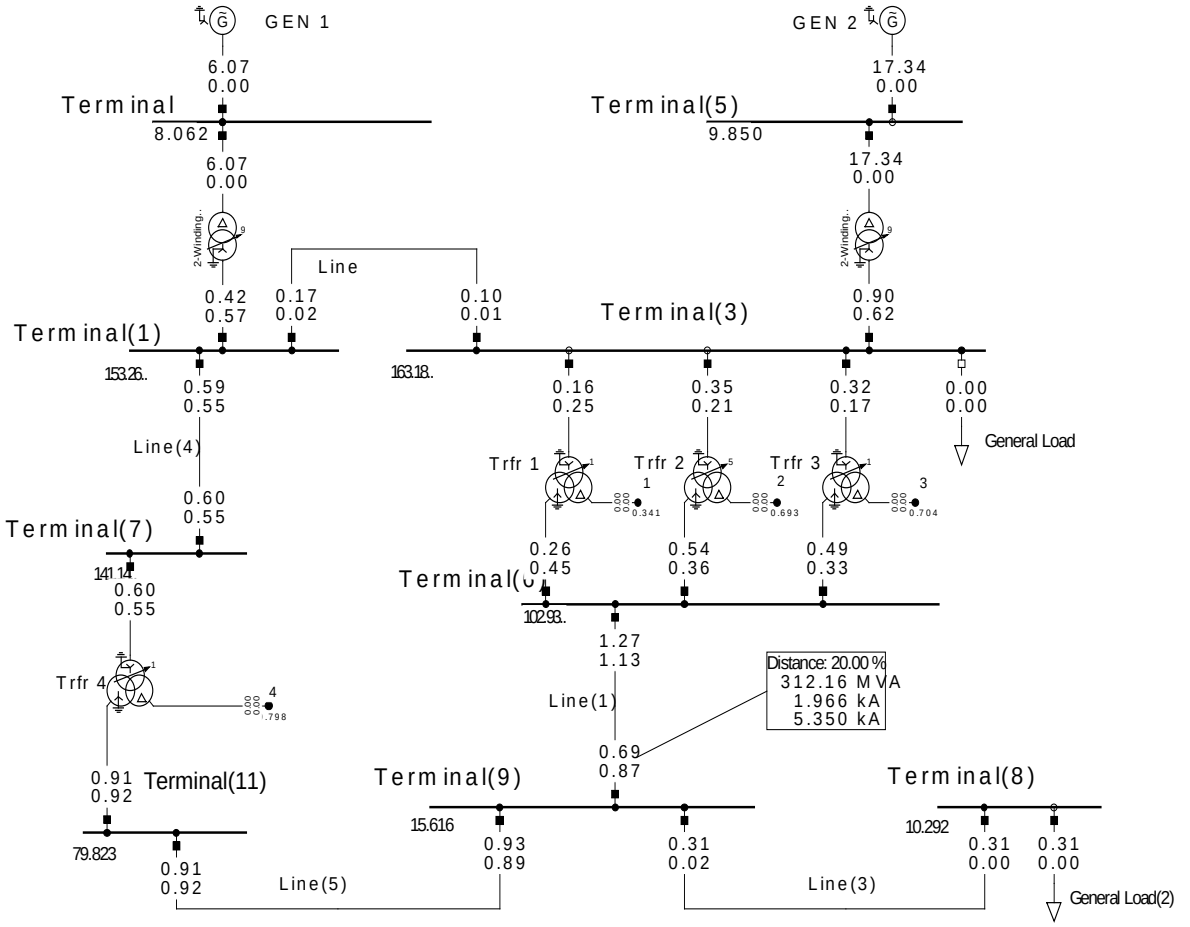

Figure 2.13: Topology illustration with single-phase fault on small network

It is possible that single-phase-to-earth faults closer to Terminal 6 will only be detected by the overreaching elements at Terminal 9. This phenomenon illustrates the importance of adequate system earthing and the need for protection permissive tripping on overhead lines. This section illustrated how the different theories can be used towards network reduction and has also shown how changes in system topology (network earthing) can impact on load and fault current distribution. These theories and methods will be utilised in Chapter 4 when the impact of system conditions on relay algorithms are evaluated. The next section will cover the principles of line impedance calculations. The importance of this section lies in the understanding of the complexity of the actual impedance of an overhead line. It will strive to highlight the various factors such as spiralling of a conductor, proximity

effect and skin effect that impacts on the overall impedance of the line and therefore also influences relay algorithm accuracy and relay settings.

Correct calculation of overhead line impedance is essential when attempting to do network simulation studies. Wrong line parameters would have a direct impact on the accuracy of simulation results obtained. Protection relay settings are calculated based on the fault and load study results obtained from such a network simulation study. It therefore follows that should the parameters used in the simulation have been calculated incorrectly, the results obtained from the studies and subsequently also the protection relay settings would be wrong. Wrong protection relay settings inevitably leads to wrong protection operation during fault conditions, resulting in unnecessary tripping of overhead lines that can lead to supply interruptions and in worst case scenarios even system instability.

2.3 Line impedance calculations from first principles

In order to have a full understanding of the equation for calculating line impedances, it is necessary to review the basics of ac-resistance, inductive reactance, conductance and capacitive reactance. J.R. Carson [4], Edith Clarke [2], William Stevenson [1] and others has developed and refined equations to calculate the impedance of high voltage overhead lines. A high degree of similarity exists between the inductance for a single conductor, a single-phase two-wire circuit, single-phase composite conductor and that for a three-phase circuit as will be illustrated in this chapter.

The intent of this section is to familiarize the reader with the equations developed by J.R. Carson et.al [1], [2] and [4]. These equations are used extensively in order to calculate line impedances. The study will focus on the resistance and inductive reactance calculations, since these quantities has a direct impact on protection relay reach measurements.

The combination of resistance and reactance are best known as the series impedance, whilst conductance and capacitance form the shunt admittance of an overhead circuit. Section 2.3 and its respective sub-sections will cover the resistance of a conductor and elaborate on various aspects that have an impact on the ac-resistance of the conductor. Section 2.3.7 and its sub-sections will discuss in detail how the inductance of overhead lines of different configurations are calculated. It will also show the relationships that exists between resistance (R) and inductive reactance (X_L) and the role of Geometric Mean Distance (GMD) as well as Geometric Mean Radius (GMR) of a conductor.

Unless explicitly stated otherwise the units of flux, inductance, resistance and temperature are in Wbt/m, H/m, Ω and °C respectively.

2.3.1 Resistance

Resistance in a network plays an important role in system damping or stability in that it is the main cause of energy losses. For protection relays the importance of resistance lies in the relationship of the network resistance versus inductive reactance that it will have to measure. More detail pertaining to the impact of system R/X ratios are discussed in Chapter 3 and Chapter 5. The resistance of an overhead line with helically-stranded conductor is dependent on the following factors [1], [13]

- Conductor resistivity
- Conductor Spiralling – lay length of aluminium layers
- Temperature
- Frequency (increased resistance due to skin effect)
- Conductor cross-sectional area
- Conductivity of the conductor
- Steel reinforced core – transformer effect as a result of magnetization due to current flow in the conductor

Resistance can be defined as a measure of the degree to which an object opposes the flow of electric current. The effective resistance of a conductor is equal to the dc-resistance of a conductor, when the distribution of current (current density) through the conductor is uniform over any cross-section, and the electric field is constant along the length of the conductor. The ac and dc-resistance (R_{ac} and R_{dc}) is then given by [1], [3] and [9]

$$R_{ac} = \frac{P_{Loss}}{I^2} \tag{2.60}$$

$$R_{dc} = \rho_v L / A \tag{2.61}$$

ρ_v =Volume resistivity of the conductor in ohm meter

L = Length of conductor in meters

A = Cross-sectional area of conductor in square meters

$$R_{dc} = \rho_m L^2 / m \tag{2.62}$$

ρ_m = *Mass resistivity of the conductor*

L = Length of conductor in meters

m = mass [2]

The dc-resistance for a stranded homogeneous conductor is given by [13]

$$\frac{1}{R_{dc}} = \frac{\pi d^2}{4\rho}\left(1 + \sum_1^n \frac{6n}{k_n}\right) \tag{2.63}$$

where

d = diameter of each strand

n = number of layers

k_n = *length factor*

$$k_n = \left[1 + \left(\frac{\pi D_n}{\lambda_n}\right)^2\right]^{1/2} \tag{2.64}$$

where

D_n = *GMR of layer n*

λ_n = *Lay length of layer*

λ_n / D_n = *Lay ratio of layer n*

For stranded steel reinforced conductors (ACSR), the dc-resistance can be obtained by [13]

$$\frac{1}{R_{dc}} = \frac{\pi d_s^2}{4\rho_s}\left(1 + \sum_1^{n_s} \frac{6n_s}{k_{ns}}\right) + \frac{\pi d_a^2}{4\rho_a}\left(1 + \sum_{n_a+1}^{n_a} \frac{6n_a}{k_{na}}\right) \tag{2.65}$$

Subscripts (a) and (s) used in Eq. (2.65) refer to the non-ferrous (non-metallic) and ferrous (metallic) sections, respectively. Variables such as resistivity, length and volume vary with temperature and as such must be selected at the same

temperature (t). When applying direct current to a multi-stranded conductor, the current density in each strand is inversely proportional to the resistivity of the strand. Uniform direct current distribution can therefore be expected for AAC (stranded aluminium conductor) or AAAC (all aluminium conductors) type conductors, but not for ACSR (aluminium conductor steel reinforced) conductors due to the variation in strand resistivity [13].

Overhead transmission line conductors are normally of the stranded type conductors. The strands of which are concentrically wound in layers around a centre strand, causing a spiralling effect in the outer layer strands. The result of spiralling is an increased resistance in the different strands due to increasing length of the individual strands, and is estimated to be 1% for three-`strand conductors and 2% for concentrically stranded conductors. The work done by Cigre' Working Group B2.12 [13] have also shown that the resistance of a conductor carrying alternating current is higher than when the same conductor carries direct current of the same magnitude for the same temperature. Cigre' Working Group B2.12 [13] had shown through the work done by others that the current distribution in the non-ferrous layers for ACSR conductors differ for the different layers and that it is influenced by the number of non-ferrous layers. It was also illustrated that the steel core in an ACSR conductor causes magnetic hysteresis and eddy current losses with resultant redistribution of current density between the subsequent non-ferrous layers of the conductor. Figure 2.14 gives an indication of the effect of stranding with increase in current for two ACSR conductors of type 54/7 and 42/7 respectively with a strand lay ratio of 13.5 *D [1], [13].

Figure 2.15 provides an indication of what can be achieved through manipulation of an ACSR type conductor strand lay ratio (lay ratio is defined as the lay length of a layer divided by the Geometric Mean Radius of that layer (λ_n/D_n)). The lay ratios were altered to obtain a minimum magnetic field in the steel core, which provided the optimal curve shown [13].

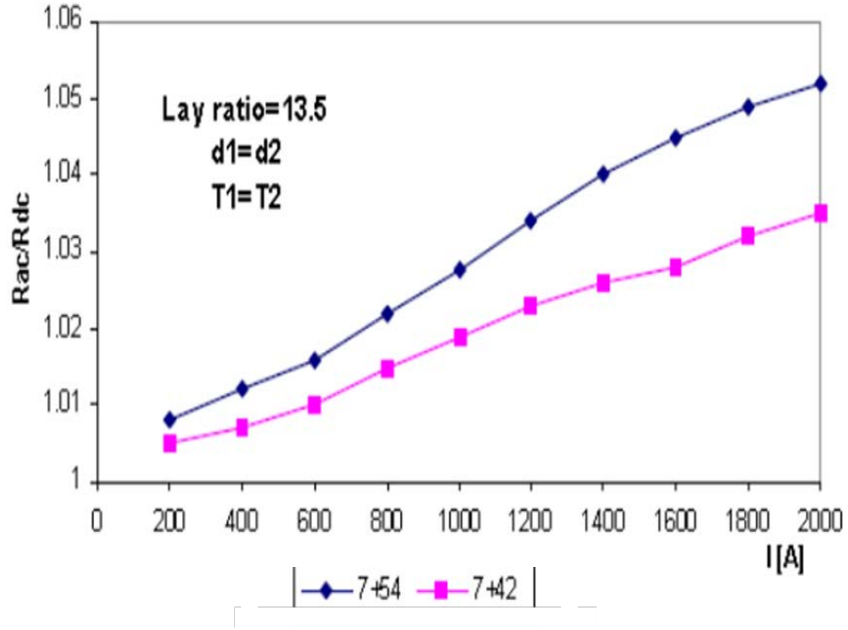

Figure 2.14: Influence of conductor stranding on ac/dc-resistance ratio [13]

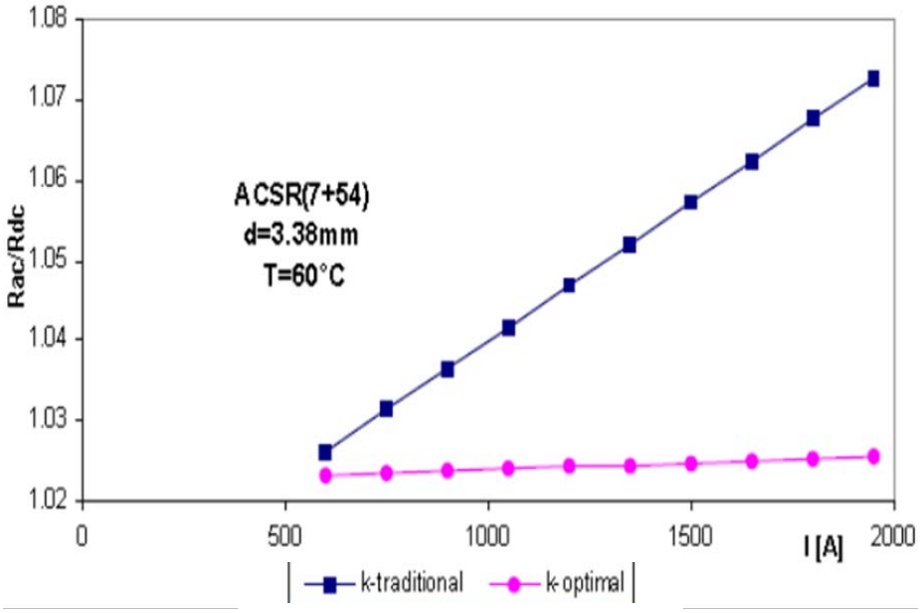

Figure 2.15: Ultimate ac/dc-resistance ratio between traditional and optimal stranding [13]

Significant variations due to the impact of conductor stranding on the ac/dc-resistance ratio can also be seen between the so-called “traditional stranded” and “optimal stranded” conductor. Since ambient temperature has an effect on the resistance of metallic conductors it is important that we know at what temperature the original conductor resistance was calculated in order to determine the resistance at any new ambient temperature.

The graph presented by Figure 2.16 can be used to determine the conductor resistance at different temperatures. Alternatively, the calculations shown below could be used [1], [2]

$$R_2 / R_1 = (T + t_2)/(T + t_1) \tag{2.66}$$

$$R_t = \rho_{20} L / A_{20}(1 + \alpha_{20}(t - 20)) \tag{2.67}$$

This equation could also be written as

$$R_t = R_0(1 + \alpha(t - T_0)) \tag{2.68}$$

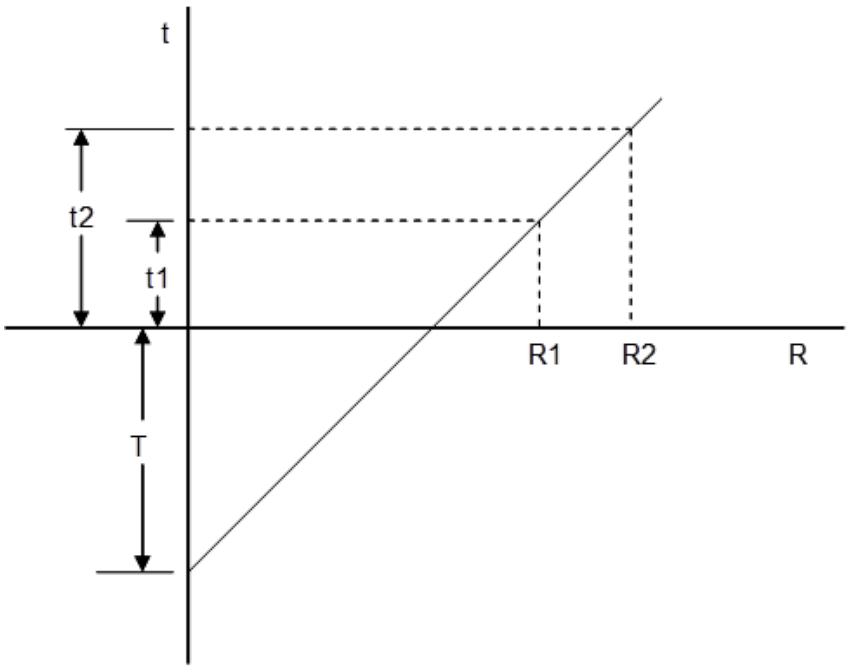

Figure 2.16: Resistance of a conductor as a function of temperature [1]

R_1 and R_2 are the conductor resistances at temperatures t_1 and t_2 respectively, with t_1 and t_2 in degrees Celsius and T being a constant for the specific conductor material. R_t is the dc-resistance at temperature t in degree Celsius, ρ the volume resistivity, L the conductor length, A the conductor cross-sectional area and α the constant mass temperature coefficient of resistance. The subscript of 20 indicates the temperature for which these values where obtained.

Typical values for T are as follows [1]

- 234.5 For annealed copper of 100% conductivity
- 241 For hard-drawn copper of 97.3% conductivity
- 228 For hard-drawn aluminium of 61% conductivity

and for α

- 0.005671 For iron
- 0.004308 For aluminium
- 0.004041 For Copper

With Eq. (2.66) only the constant for the specific conductor material (T) is required to calculate resistance at different temperatures. This is an approximated calculation where it is accepted that the variation of the resistance of metallic conductors is linear over the normal temperature operating range. Eq. (2.67) takes into account the variations of length, conductor cross-section and the constant mass temperature coefficient of resistance at the specific conductor operating temperature for which a calculation is required. Substantially more accurate values for different operating temperatures would therefore be obtained with Eq. (2.67).

The resistance of ferrous type conductors, such as steel, are directly proportional to the magnitude of current, the development of internal flux linkages and internal magnetic losses. In order to obtain the correct ac-resistance it is therefore essential to utilize a calculation method, which will take all the factors of temperature, stranding, wire diameter, developing fluxes and internal magnetic losses into account [13]. Figure 2.17 presents a relationship in an ACSR type conductor for conductor resistance versus temperature changes as obtained from [19].

Cigre' Working Group B2.12 [13] has suggested two methods of calculating conductor ac-resistance of stranded conductors. The first method is based on the work done by Barret et al and uses a MathCAD program developed to determine the ac-resistance for a given current [13]. The second method was developed by

Güntner and Varga according to Cigre' Working Group B2.12 [13] and also provided a computer program to determine the ac-resistance.

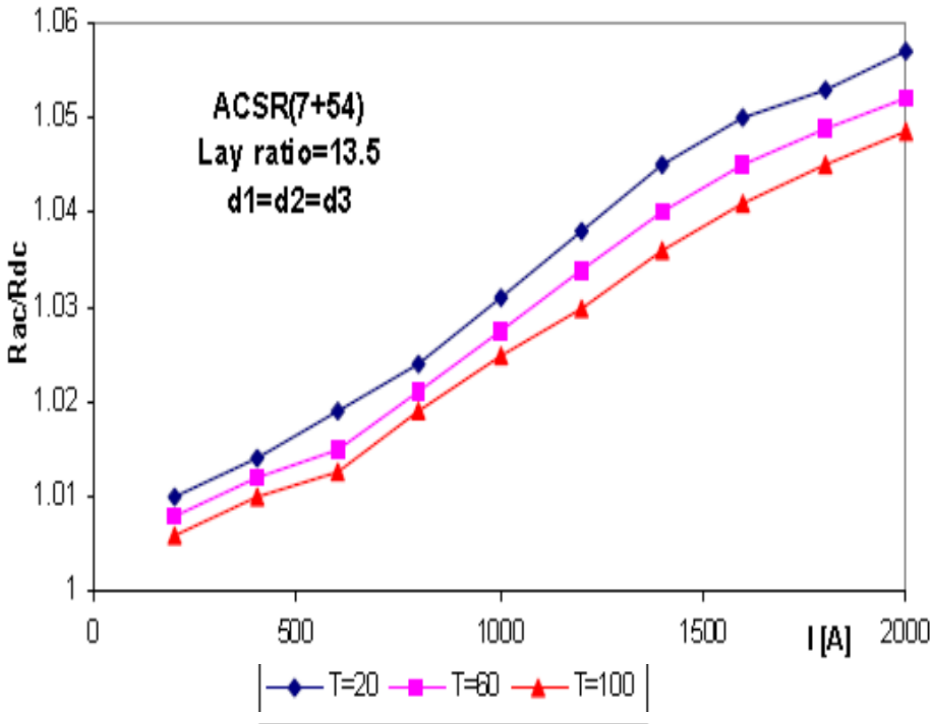

Figure 2.17: Resistance variations based on temperature and current [13]

The workgroup also determined that the ac-resistance of overhead line conductors of the type AAC or AAAC can be calculated with good accuracy taking into account the conductor geometry and other factors such as skin effect, current density, spiralling and proximity effect. Conductors of type ACSR, require more complex calculations due to the magnetic flux interactions caused by the currents in each layer coupled through the steel core [13].

Figure 2.18 provides a graphical view of the differences in ac-resistance increase per type of conductor. The magnetic flux interactions, or more commonly referred to as the transformer effect, induces currents in the layers as a result of the magnetization of the steel core. The result is a higher current density in the middle layer of a three-layer aluminium conductor [13], highlighting the fact that more current will be flowing in the outer layers than in the steel core. In fact, the alternating magnetic flux created in the core will result in eddy current and hysteresis losses in the core and will impact the current distribution in all other aluminium layers. In conductors with

identical stranding in all layers the most important factors influencing ac-resistance are the skin and temperature effects [13].

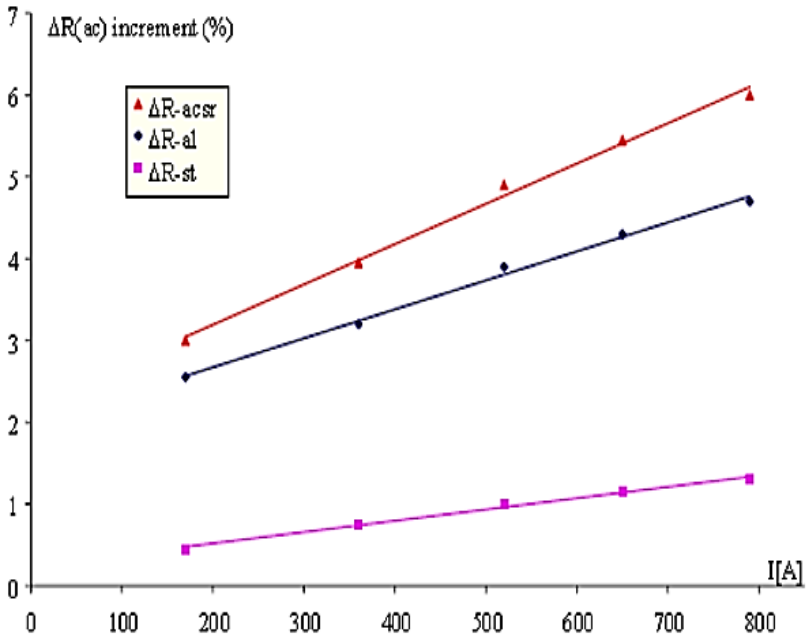

Figure 2.18: Variation in ac-resistance per type of conductor [13]

2.3.2 Skin effect

Skin effect results in an effective increase in the ac-resistance of a conductor and a decrease in its internal inductance, whilst it does not influence the conductor external inductance [2]. Non-uniformity of current distribution throughout the cross-section of a conductor in a multilayer conductor is directly proportional to the alternating frequency of the current passing through the conductor. An increase in frequency results in an increase in non-uniformity of current distribution in the conductor. A higher current density closer to the surface of the conductor with reference to the centre of the conductor is obtained at increasing frequencies, resulting in an effective reduction in cross-section of the conductor and therefore higher conductor resistance.

This phenomenon is the direct result of self-induced voltages (emf's) in the conductor due to the varying magnetic flux created by the alternating current flowing in the conductor. The increase in current density closer to the outer radius of the

conductor, symmetrical about the axis of a cylindrical conductor, is referred to as the skin effect [1], [3], [13]. Figure 2.19 shows the laboratory test results obtained by Cigre' Working Group B2.12 [13]. Non-uniformity of the current distribution in a multi-stranded conductor is graphically explained with the aid of Figure 2.20. The induced voltages represented by U_{i1}, U_{i2} and U_{i3} results in the overall current distribution as shown. The second layer therefore has a total current of $I_{A1} + I_{A11}$, whilst the first and third layers only have currents I_{A1} and I_{A11} respectively.

The impact of nominal power frequencies on conductor resistance can be ignored with all aluminium-stranded conductors, however this is not so with steel reinforced conductors, because of the forced re-distribution of current in the different layers as well as the losses in the steel core. The direction of the fluxes created by the induced currents are in opposing directions in the different layers due to the different stranding directions of the different layers of strands in the conductor. This has the result that the induced voltage and current in the middle layer of the conductor is greater than that for the inner or outer layer [13].

The current densities in the different layers of an ACSR type conductor are reflected by the designations of J_1, J_2, J_3 and J_{st} in Figure 2.19 for the relevant aluminium layers and steel core respectively. J_h reflects the average current density in the aluminium layers alone. Different percentage increases in ac-resistance results due to the skin effect and has been shown to be [13]

- Between 1% and 10% for conductors of diameters 20 mm to 50 mm
- Between 5% to 20% for single and three-layer ACSR conductors

Cigre' Working Group B2.12 [13] has listed the following factors that impact the resistance measurement of a conductor negatively

- Effectiveness of the electrical contact with all layers of the conductor – compression glands should provide the best contact.
- Degree of conductor strand oxidation and tension in the conductor determines the electrical contact between strands.

- Radial and longitudinal temperature gradient in the conductor, since it is not isothermal.

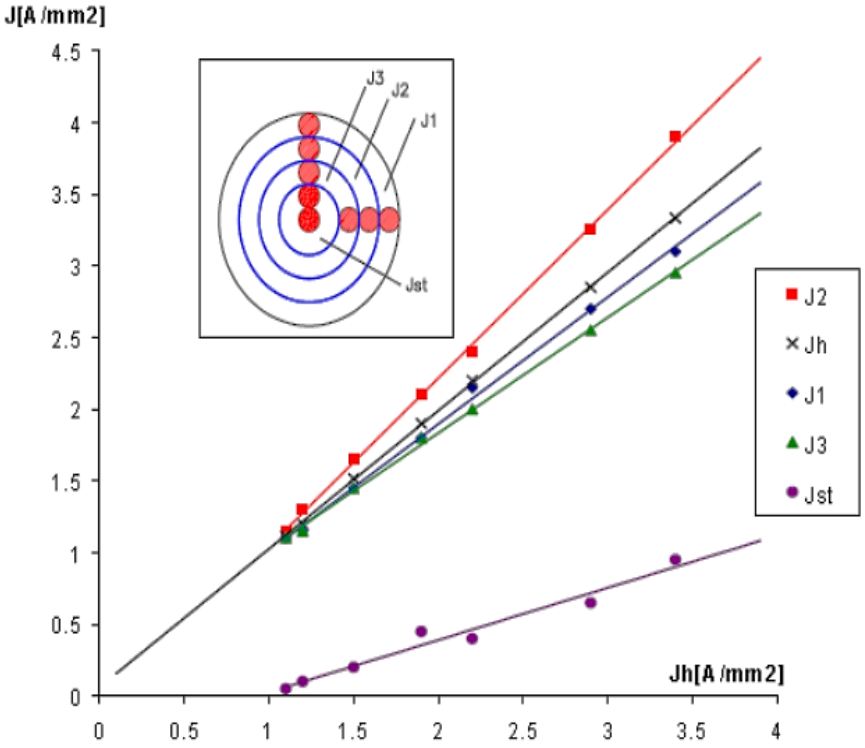

Figure 2.19: Increase in current density per layer [13]

Skin effect, although independent of circuit configuration and sequence of current, is influenced by the frequency, type of material and physical dimensions of the conductor [2]. Equations for skin effect resistance and inductance ratios for bolted homogeneous cylindrical conductors of constant permeability have been developed by Edith Clarke [2] and are reflected in its simplified format in Eq. (2.69), Eq. (2.70) and Eq. (2.71). According to Edith Clarke, using the equation for the calculation of x in Eq. (2.71), negates the necessity of considering conductor resistivity and dimension changes due to temperature.

Resistance ratio [2]

$$\frac{R'}{R_{dc}} = \frac{x}{2\sqrt{2}} + \frac{1}{4} \tag{2.69}$$

Inductance ratio [2]

$$\frac{L_i'}{L_i} = \frac{2\sqrt{2}}{x} \tag{2.70}$$

The value of x is defined as [2]

$$x = 0.02768\sqrt{\frac{f\mu}{R_{dc}}} \tag{2.71}$$

where

R_{dc} = dc-resistance of conductors at specific temperature

R' = effective ac-resistance inclusive of skin effect

L_i = internal conductor inductance assuming uniform current distribution

L_i' = internal conductor inductance inclusive of skin effect

μ = *conductor permeability*

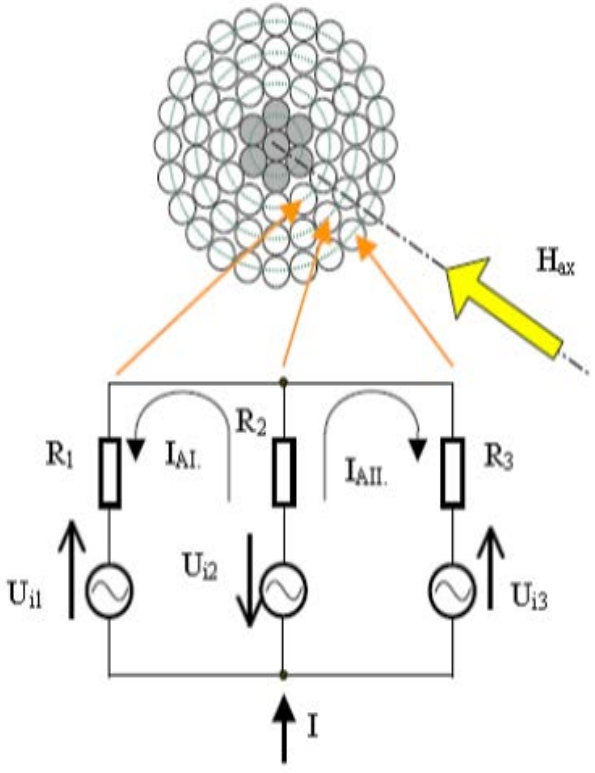

Figure 2.20: Theoretical explanation for uneven current distribution in ACSR conductors [13]

The skin effect resistance and inductance ratios can also be obtained from graphs developed by Edith Clarke and Dwight [2], [8]. Figure 2.21 shows the curves developed by Dwight. The impact of frequency on the conductor ac to dc-resistance ratio, based on the outer radius of the conductor inner steel core and the outer radius of the last aluminium layer, can be determined from Figure 2.21. In order to determine the value of x in Eq. (2.71), the value of conductor permeability (μ) needs to be obtained for the different types of conductors used. The permeability values for different conductors should be obtained with the same reference in terms of current, frequency and manufacturing processes due to the influence that these variables has on conductor permeability.

The internal impedance inclusive of Skin effect of a conductor can then be obtained from Eq. (2.72) [2]

$$Z_i = R_{dc} \cdot \frac{R'}{R_{dc}} + jX_i \cdot \frac{L_i'}{L_i} \tag{2.72}$$

The value for dc-resistance (R_{dc}) and internal inductance (X_i) can be obtained from manufacturers tables or the internal inductance can be calculated from the general equation $X_i = 2\pi fL$ [2]. No further attention will be given to the above method, but calculation methods used by J.R. Carson et.al still in use today will be explored in sections to follow. The position of current flow inside the conductor, a phenomena also know as Skin depth will be explored in section 2.3.2.1.

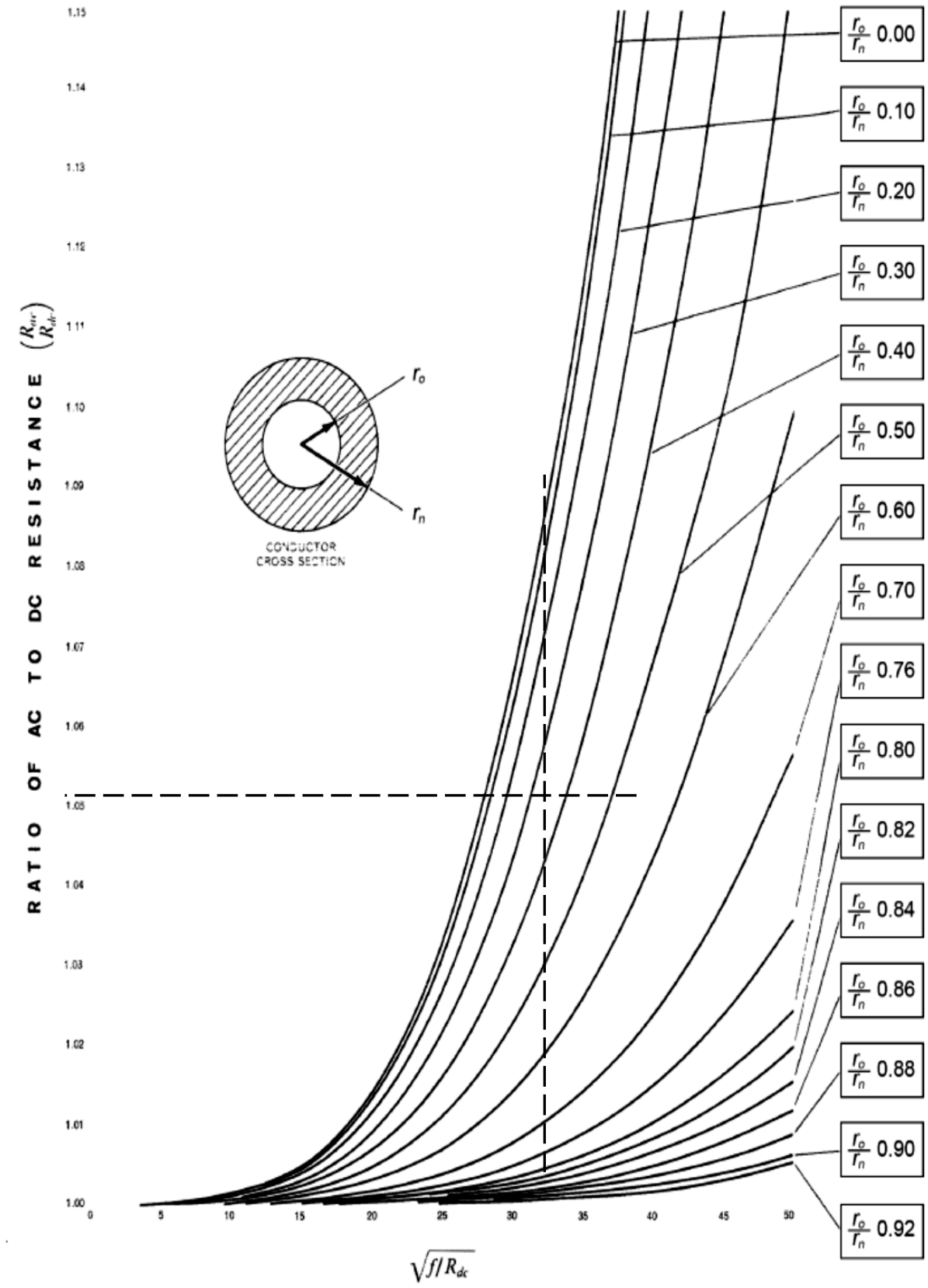

Figure 2.21: Skin effect curves for bolted round bare stranded conductor [8]

2.3.2.1 Skin depth

Based on the skin effect phenomenon described in detail in section 2.3.2, it is clear that current density decays towards the centre of an ACSR conductor. This uneven distribution of current through a conductor results in an increase in its ac-resistance. At a certain so-called skin depth the current decays to 1/e (e = 2.71828) of the current density at the surface of the conductor. Eq. (2.73) provides the skin depth in mm [8]

$$d = \sqrt{\frac{2\rho}{\omega\mu}} \tag{2.73}$$

where

ρ = resistivity of conductor

ω = angular frequency of current = $2\pi f$

μ = absolute magnetic permeability of conductor

Skin depth has also been formulated in by Ramo, Whinnery and Van Duzer [4] as

$$d_s = \frac{1}{\sqrt{\pi\mu_0}}\sqrt{\frac{\rho}{\mu_r f}} \tag{2.74}$$

where

$\mu_0 = 4\pi * 10^{-7}$

μ_r = *relative permeability of conductor*

f = *frequency*

The typical value of relative permeability for non-magnetic conductor material such as copper and aluminium is as assumed to be 1.

2.3.2.2 Current density

The current density, referred to in section 2.3.2.1, as defined for an infinitely thick conductor, decreases exponentially from the surface to the centre of the conductor due to the skin effect and can be calculated using the following equation

$$J = J_s e^{-\delta/d} \tag{2.75}$$

where

J = current density at depth δ from the conductor surface

J_s = current density at the conductor surface

δ = depth from conductor surface

d_s = skin depth

2.3.3 Proximity effect

The ac-resistance of a conductor is further influenced by a phenomenon called the proximity effect. The proximity effect occurs on high voltage lines and causes non-uniform current distribution over the cross-section of the conductors. This effect is the direct result of changing current in conductors in close proximity. Whilst the non-uniform current distribution caused by the skin effect is symmetrical around the axis of symmetry of a round conductor, that caused by the proximity effect is unsymmetrical [2].

Proximity effect differs from skin effect in that it is dependent on circuit configuration, magnetic flux distribution in and outside the conductor, current magnitude and phase (angular) relationships between currents in the different conductors in close proximity. Since the phase relationship between currents influences the proximity effect, it can be concluded that this effect will be different for positive and zero sequence currents in the same circuit. Whilst the skin effect only influences the internal resistance and inductance of a conductor, the proximity effect changes the internal resistance as well as the total inductance (internal + external) of the conductor [2].

The inner and outer magnetic flux distribution can be calculated for each layer in a conductor if the initial assumption of uniform current density per layer is made. The magnetic flux can then be calculated using the following equations [13]

$$\varphi_{n,outer} = \frac{1}{2\pi}\left(I_s + I_1 + \ldots k_1 I_n\right)\mu_0 \ln\left(\frac{D_n}{\left(D_n - d\right)}\right) \tag{2.76}$$

$$\varphi_{n,inner} = \frac{1}{2\pi}\left(I_s + I_1 + \ldots k_2 I_n\right)\mu_0 \ln\left(\frac{\left(D_n - d\right)}{\left(D_{n-1}\right)}\right) \tag{2.77}$$

where

$\varphi_{n,\ outer}$ = Outer magnetic flux associated with each layer

$\varphi_{n,\ inner}$ = Inner magnetic flux associated with each layer

I_s = Current in the steel core

I_1 … I_n = Current in the different layers

μ_0 = permeability of free space

k_1 = Coefficient of current concentration (specific to conductor type)

k_2 = Coefficient of current concentration (specific to conductor type)

D_n = Geometric Mean Radius (mean diameter) of layer n

d = Diameter of each strand

From this the inner and outer inductive reactance per conductor layer can be calculated as follows [13]

$$X_{n,outer} = j \cdot f\mu_0\varphi_{n,outer} \tag{2.78}$$

$$X_{n,inner} = j \cdot f\mu_0\varphi_{n,inner} \tag{2.79}$$

where

$X_{n,outer}$ = Outer mutual inductive reactance

$X_{n,inner}$ = Inner mutual inductive reactance

f = Frequency

A reduction in spacing between conductors results in a decrease in the total inductance to neutral of the conductor. Non-uniform current distribution caused by

the proximity of conductors is said to have a lesser impact on the inductance of the conductor than on the resistance of the same conductor. At “low” power system frequencies the proximity effect on the inductance for non-magnetic circuits in a similar environment, is normally considered insignificant are therefore ignored [2], [13].

2.3.3.1 Resistance and inductance relationships

In an attempt to simplify overhead conductor impedance calculations, using skin effect and proximity effect, Edith Clarke defined the following relationships for resistance and inductance [2]

Skin effect resistance ratio = R'/R_{dc}
Proximity effect resistance ratio = R''/R'
Effective ac-resistance: $R_{ac} = R_{dc}.R'/R_{dc}.R''/R'$
Skin effect internal inductance ratio = L'_i/L_i
Internal inductance with skin effect: $L'I = L_i.L'_i/L_i$
Inductance to neutral with skin effect: $L' = L_e + L'_i$
Proximity effect inductance ratio = L''/L'

Total inductance to neutral L” (Skin- and proximity effect included)

$$L'' = L' \cdot \frac{L''}{L'} \tag{2.80}$$

$$L'' = \left(L_e + L_i'\right) \cdot \frac{L''}{L'} \tag{2.81}$$

where

R_{dc} = dc-resistance of conductors at specific temperature
R_{ac} = ac-resistance of conductors at specific temperature
R’ = effective ac-resistance inclusive of skin effect
R” = Total effective ac-resistance inclusive of skin and proximity effect
L_i = internal conductor inductance assuming uniform current distribution

L_e = external conductor inductance to neutral assuming uniform current distribution

L'_i = internal conductor inductance inclusive of skin effect

L' = conductor inductance to neutral inclusive of skin effect

L" = total conductor inductance to neutral inclusive of skin and proximity effect

It should be noted that the proximity effect can be ignored when the conductors are spaced far apart. The ratios of R"/R' and L"/L' can then be set to unity, with the resultant conductor inductance being equal to the inductance to neutral inclusive of the skin effect only. Transmission overhead circuits are normally designed such that the conductors are spaced far apart. Proximity effect then plays an insignificant role, and can be ignored.

2.3.4 Spiralling effect

Another cause of change in conductor ac-resistance has been the spiralling of conductor strands. Spiralling of strands to form a composite conductor with the exception of the centre strand, results in the individual strands being longer than the conductor itself. This individual strand length is also referred to as lay length [13]. In order to prevent unwinding of the strands of a conductor, alternate layers of strands are spiralled in opposite directions. This also ensures that the outer radius of the inner layer of strands coincide with the inner radius of the next layer of strands, a factor which for non-spiralled composite conductors has shown the skin effect resistance and internal inductance ratios to be the same as for a solid conductor of the same material and cross-section. Variations in the internal inductance ratios are therefore caused by spiralling of the different layers of conductor strands [1], [2].

2.3.5 Transformer effect

The ac-resistance of an ACSR conductor is further impacted by a phenomenon called the "Transformer effect". This effect is a direct cause of the steel reinforced core that is used in this type of conductor. Different equivalent circuit models exist to determine the effect of the steel core in ACSR conductors, but these models associated the core loss with each layer of the conductor assuming non-uniformity of current in the different layers. Latest studies done by Cigre' Working Group B2.12

[13] have included the total impact of the magnetic fluxes that develops in the core and has developed the following equations to calculate the complex self-inductive reactances of the different layers of aluminium strands due to this flux.

$$X_{nn} = 2\pi f \mu_0 \left[\left(\left(\frac{\pi}{4} \right) D_n^2 - A_s \right) + \mu_r A_s \right] / \lambda_n^2 \tag{2.82}$$

The complex mutual inductive reactances calculated with the use of

$$X_{pq} = 2\pi f \mu_0 \left[\left(\left(\frac{\pi}{4} \right) D_p^2 - A_s \right) + \mu_r A_s \right] / \lambda_p \lambda_q \tag{2.83}$$

and

$$X_{qp} = X_{pq} \tag{2.84}$$

where

X_{nn} = Complex self-inductive reactance of the nn-th layer

X_{pq} = Complex mutual inductive reactance of the nn-th layer

D_n = Mean diameter (GMR) of layer n

D_p = Mean diameter (GMR) of layer p

λ_p and λ_q are the lay lengths of layers p and q

μ_r = Relative permeability of the conductor

A_s = Cross section area of the steel core

2.3.6 Magnetic permeability

All of the factors that can influence the ac-resistance of an overhead conductor have now been explored. Before the inductance of the conductor can be discussed, it is important to understand the concept of magnetic permeability. Permeability forms an integral part of the algorithms required to calculate the inductance of a conductor. The permeability of vacuum in ampere per meter, illustrated in Figure 2.22 and mathematically represented by Eq. (2.85), is obtained from observing the magnetic field strength (H), due to the current in one conductor, and the magnetic flux density

(B) caused by the applied current in two long straight conductors (A and C), both carrying one ampere, running in parallel and spaced 1 meter apart in vacuum [1].

The relationship between magnetic field strength and current can be written as [1]

$$H = \frac{I}{d} = \frac{I}{2\pi r} \tag{2.85}$$

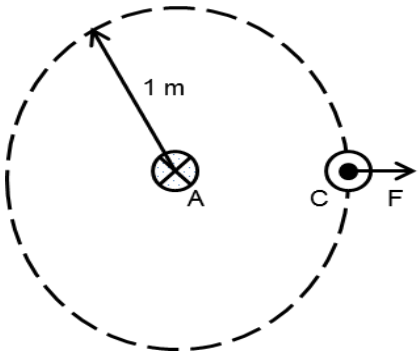

Figure 2.22: Magnetic field strength of two conductors in parallel

The relationship for magnetic flux density (B) measured in tesla is obtained from the Biot-Savart law.

$$B = 2 \cdot k' \frac{I}{r} \tag{2.86}$$

$$k' = \frac{\mu_0}{4\pi} \tag{2.87}$$

where

I = current in conductor

d = path length of magnetic field line

r = radial distance of point P from the conductor

The magnetic permeability for vacuum (μ_0), measured in weber per ampere-meter, is obtained from the relationship between the magnetic flux density (B) and the magnetic field strength (H) [1].

$$\mu_0 = \frac{B}{H} \tag{2.88}$$

therefore

$$\mu_0 = 2k' \frac{I}{r} \cdot \frac{2\pi r}{I} \tag{2.89}$$

$$\mu_0 = 4\pi \cdot 10^{-7} \tag{2.90}$$

The permeability of specific mediums such as steel, air, aluminium etc. is normally referred to as absolute permeability. The absolute permeability of magnetic materials is dependent on magnetic field strength and temperature, whilst that for most non-magnetic materials is not, and is almost equal to the permeability for vacuum. Relative permeability (μ_r) is then defined as the ratio between the absolute permeability of the material and the permeability for vacuum [1].

$$\mu_r = \frac{\mu}{\mu_0} \tag{2.91}$$

2.3.7 Inductance of a conductor

We have seen from the discussions above that the total inductance of a conductor is dependent on various factors such as the current frequency, skin effect, proximity and spiralling of the conductor. Inductance is defined as the property of a circuit that relates the voltage induced by a changing flux to the rate of change of current flowing in the circuit [1].

Two fundamental voltage equations are used to define inductance [1]

$$e = \frac{d\varphi}{dt} \tag{2.92}$$

and

$$e = L\frac{di}{dt} \tag{2.93}$$

where

e = induced voltage

φ = number flux linkages of a circuit in weber-turns

L = inductance of the circuit

$d\varphi/dt$ = rate of change of flux

di/dt = rate of change of current

The inductance in Henry can now be obtained from the above equations as [1]

$$L = \frac{d\varphi}{di} \tag{2.94}$$

The inductance of a transmission line is influenced by the internal and external flux associated with each conductor. The inductance of a transmission line differs on a per phase basis dependent on the conductor positioning in relation to each other due to the internal and external fluxes that develop as a function of the current in each conductor. Consequently, due to non-equilateral spacing of conductors normally used on high voltage overhead lines, the different phases of the circuit will each have its own unique inductance. This is due to the difference in the external flux linkages that exists between the different phases. The difference in flux linkage and hence in inductance per phase could be overcome with the use of transposition [2].

Unsymmetrical current distribution within the conductor and the resulting magnetic flux distribution around the axis of different conductors are directly related to the proximity of the conductors. A closer proximity will result in an increase in unsymmetrical current and magnetic flux distribution. In a flat conductor spacing relationship, the centre phase will therefore have the highest degree of unsymmetrical current and magnetic flux distribution, resulting in a higher degree of change in its ac-resistance and inductance in comparison to the outer phases [2].

To determine the internal inductance of a conductor we first need to determine the total internal flux. Consider the cross-section of a cylindrical conductor shown in Figure 2.23 below. The magneto motive force, magnetic field intensity, flux density and finally the flux linkages per meter length, caused by the flux in the tubular

section, x meters away from the centre of the conductor can be calculated. Since the external flux links all the current in the conductor only once, the change in flux linkages ($d\psi$) per meter are numerically equal to the change in flux ($d\varphi$) [1]. For consistency, only the variable φ will be used in all equations quoted. Through integration from the centre of the conductor to the outside radius the total flux linkages (φ_{int}) inside the conductor are obtained [1].

$$\varphi_{\text{int}} = \int_0^r \left(\frac{\mu I x^3}{2\pi r^4} \right) dx \tag{2.95}$$

and

$$\varphi_{\text{int}} = \frac{\mu I}{8\pi} \tag{2.96}$$

where

I = current in conductor

r = radius of the conductor

μ = absolute magnetic permeability of the conductor or $\mu_a = \mu_r . \mu_0$

It is therefore important to note that the internal flux would be different for different types of conductor materials used, since the absolute magnetic permeability characteristics are different.

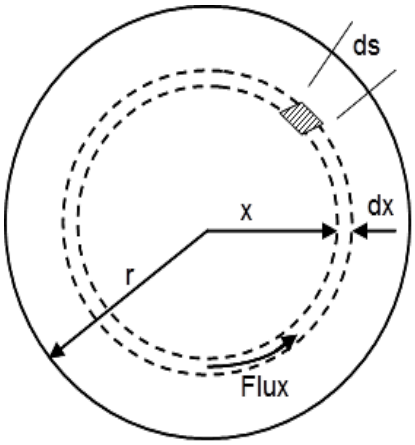

Figure 2.23: Cross-section of a cylindrical conductor [1]

The degree of magnetization of a specific material, which is linear to the applied magnetic field, is defined as the permeability of the material and is represented by the Greek letter μ.

The permeability of aluminium is the same as that for air or vacuum as shown in Appendix L. For aluminium conductors the value of permeability used is therefore equal for both the internal and external inductance calculations. The external inductance is the inductance in free space around the conductor caused by the external magnetic flux generated by the alternating current in the conductor. The internal and external inductance referred to here is the self-inductance of the conductor, and must not be confused with the mutual inductance, which is caused by the flux linkages from the currents flowing in other nearby conductors. This is not true for steel or other combinations of Ferro-metal conductors.

The internal inductance for steel or other combinations of Ferro-metal conductors must be calculated using the specific materials permeability value, 875 $\mu N/A^2$ (see Appendix L) for steel, whilst the external inductance for the steel conductor is calculated using the permeability value for air. The relative permeability for aluminium is given by the ratio of absolute magnetic permeability for aluminium versus the permeability for air. ($\mu_r = \mu/\mu_o = 1$).

For a relative permeability of 1 ($\mu = 4\pi \times 10^{-7}$), the total internal flux linkage is therefore

$$\varphi_{\text{int}} = \frac{1}{2} I * 10^{-7} \tag{2.97}$$

It can be shown that

$$\varphi = LI \tag{2.98}$$

The internal inductance of a conductor in Henry per meter is then [1]

$$L_{\text{int}} = \frac{1}{2} * 10^{-7} \tag{2.99}$$

J.R. Carson has represented the internal inductance with the following equation [8]

$$L_i = \frac{\mu_0}{2\pi} \cdot \ln\left(\frac{r}{re^{-\mu_r/4}}\right) \tag{2.100}$$

This relationship calculates to the same numerical value as is given by Eq. (2.99). Similarly the total external flux linkages per meter of conductor length can be obtained. Assuming that other current carrying conductors are at a distance far enough away, so as not to influence the flux distribution in and around this conductor, the external flux can be shown to exist in concentric circles around the conductor (see Figure 2.24). The change in flux is given by Eq. (2.101).

$$d\psi = d\varphi = \frac{\mu_0 I}{2\pi x} dx \tag{2.101}$$

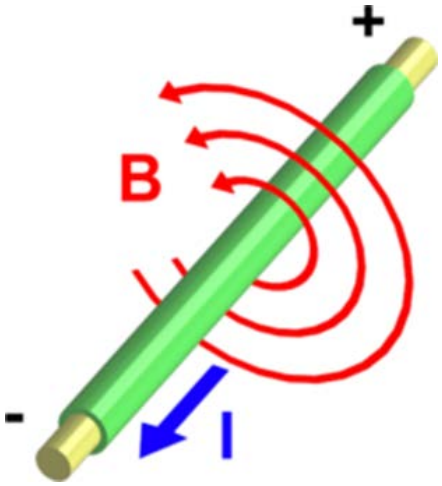

Figure 2.24: Current (I) flowing through a conductor produces a magnetic field (B) around the conductor [3]

The total external flux linkages are obtained through integration between points P1 and P2, defined as the area containing all the relevant external flux. The distance between the centre of the conductor and points P_1 and P_2 is given as D_1 and D_2 respectively (see Figure 2.25).

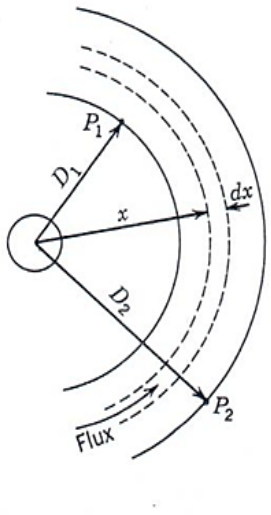

Figure 2.25: External magnetic flux between points P1 and P2 for a single conductor [1]

The total external flux in Weber turns/meter is [1]

$$\varphi_{ext} = \frac{\mu_0 I}{2\pi} \ln\left(\frac{D_2}{D_1}\right) \tag{2.102}$$

The total external inductance in H/m is then

$$L_{ext} = 2*10^{-7} \ln\left(\frac{D_2}{D_1}\right) \tag{2.103}$$

The total self-inductance for the conductor with relative permeability of 1 can now be calculated from [1]

$$L_{tot} = L_{\text{int}} + L_{ext} \tag{2.104}$$

hence

$$L_{tot} = 2*10^{-7} \ln\left(\left(\frac{D_2}{D_1.e^{-\frac{1}{4}}}\right)\right) \tag{2.105}$$

To determine the total inductance for a conductor with relative permeability not equal to 1, the value of μ_0, as used for internal inductance for copper or aluminium conductors with $\mu_r = 1$, must be replaced with the absolute permeability of the conductor as in Eq. (2.96) for the internal inductance. The following equations can then be derived

$$L_{\text{int}} = \frac{\mu}{8\pi} \tag{2.106}$$

and

$$L_{ext} = \frac{\mu_0}{2\pi} \ln\left(\frac{D_2}{D_1}\right) \tag{2.107}$$

therefore

$$L_{tot} = \frac{\mu}{8\pi} + \frac{\mu_0}{2\pi} \ln\left(\frac{D_2}{D_1}\right) \tag{2.108}$$

(For simplicity, all equations shown later in this document, unless otherwise stated, will assume a relative permeability equal to 1.)

2.3.7.1 Inductance of a single-phase two-wire line

For a single-phase two-wire line the total inductance of the circuit is the combination of the internal and external inductances caused by the currents in both conductors. It is important to note that as a prerequisite the vector sum of the two currents must equal zero. The calculation of the internal inductance of a conductor has already been shown. The external inductance of a dual conductor circuit differs ever so slightly from that for a single conductor, in that the points defining the total external flux are the radius of the conductor, and the distance between the centres of the two conductors. D_2 and D_1 in the equation for a single conductor are replaced by D and r, where r could be the radius of conductor one or two (see Figure 2.26).

Flux created by the alternating current in conductor one, which is at a distance equal to or greater than the distance (D) between the conductors plus the radius (r_2) of conductor two, will link a total current of zero and will therefore not induce a voltage

into either conductor. The number of lines of flux linking conductor 1 varies from 1 before crossing the surface of conductor 2 to 0 after crossing conductor 2. It therefore follows that should a uniform current density exist in both conductors, the maximum radius for external flux for any one of these conductors can be defined as the distance between the centres of the conductors [1].

This point will be further illustrated when the same equation is derived using a distant point P as reference in the calculation of the total magnetic flux generated. Let L_1 and L_2 provide the total inductance for the two individual conductors.

Self-inductance for conductor 1 [1]

$$L_1 = 2 \cdot 10^{-7} \ln\left(\frac{D}{r_1 \cdot e^{-1/4}}\right) \tag{2.109}$$

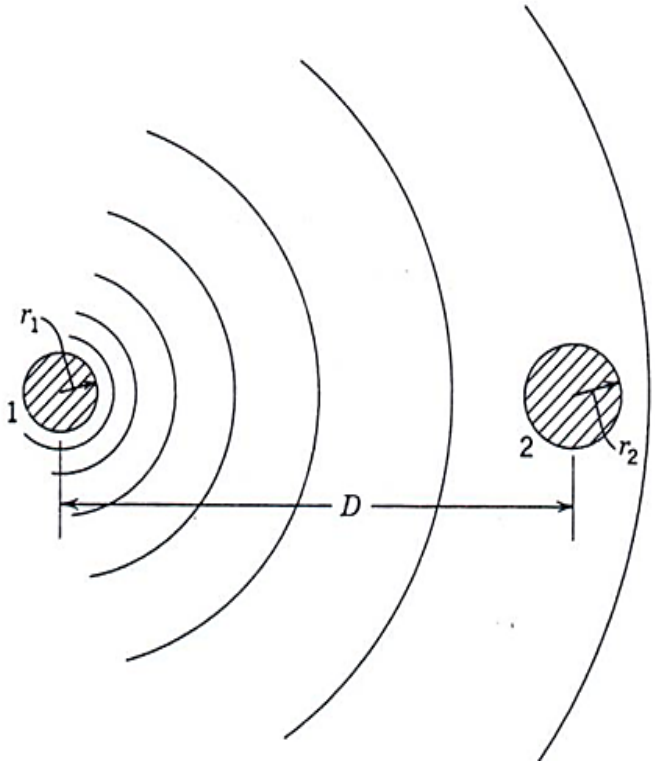

Figure 2.26: Field due to current in conductor 1 only [1]

Self-inductance for conductor 2 [1]

$$L_2 = 2 \cdot 10^{-7} \ln\left(\frac{D}{r_2 \cdot e^{-1/4}}\right) \tag{2.110}$$

The total inductance for the single-phase circuit can then be calculated as [1]

$$L_{tot} = L_1 + L_2 \tag{2.111}$$

$$L_{tot} = 4 \cdot 10^{-7} \ln\left(\frac{D^2}{r_1 \cdot e^{-1/4} \cdot r_2 \cdot e^{-1/4}}\right) \tag{2.112}$$

Now, if the two conductors have equal radius, then $r_1 = r_2 = r$, and we can simplify the above equation by assigning $r' = r.e^{-1/4}$. Therefore [1]

$$L_{tot} = 4 \cdot 10^{-7} \ln\left(\frac{D}{r'}\right) \tag{2.113}$$

The total inductance (L_{tot}) when the relative permeability of the conductor is not equal to 1 can be derived from first principles as

Self-inductance for conductor 1

$$L_1 = \frac{1}{8\pi}\left(\mu_1 + 4\mu_0 \ln\left(\frac{D}{r_1}\right)\right) \tag{2.114}$$

and

Self-inductance for conductor 2

$$L_2 = \frac{1}{8\pi}\left(\mu_2 + 4\mu_0 \ln\left(\frac{D}{r_2}\right)\right) \tag{2.115}$$

Total inductance for the circuit if $r_1 = r_2$ and $\mu_1 = \mu_2$

$$L_{tot} = \frac{1}{4\pi}\left(\mu + 4\mu_0 \ln\left(\frac{D}{r}\right)\right) \tag{2.116}$$

The relevance of using the above equation becomes apparent when conductors of different materials not having the same permeability as that for air are used. To determine the external flux generated by the currents in the different conductors an arbitrary point P in space is chosen. The equation for the calculation of the magnetic flux due to the current in conductor 1 has already been shown above. By replacing D with D_{1P} and D_{2P} respectively, the following equations are obtained for the flux associated with conductor 1 due to the current in conductors 1 and 2 [1]

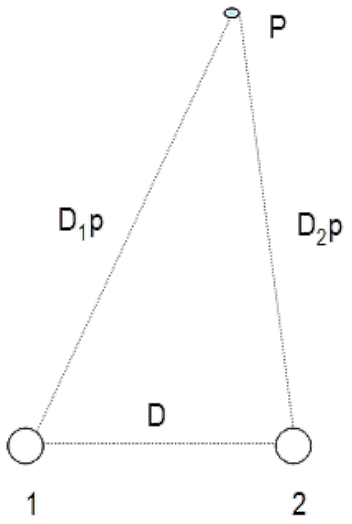

Figure 2.27: Single-phase circuit inductance calculation with reference to point P [1]

Equations derived using reference point P in Figure 2.27.

Flux for conductor 1 due to current in conductor 1 (Self-induced) [1]

$$\varphi_{1P1} = 2 \cdot 10^{-7} I_1 \ln\left(\frac{D_{1P}}{r_1 \cdot e^{-1/4}}\right) \tag{2.117}$$

Flux for conductor 1 due to current in conductor 2 (Mutually coupled) [1]

$$\varphi_{1P2} = 2 \cdot 10^{-7} I_2 \ln\left(\frac{D_{2P}}{D}\right) \tag{2.118}$$

Total flux for conductor 1 (Self and mutual) [1]

$$\varphi_1 = \varphi_{\text{int}} + \varphi_{ext} + \varphi_{mutual} \tag{2.119}$$

$$\varphi_1 = 2 \cdot 10^{-7}\left(I_1 \ln\left(\frac{1}{r_1'}\right) + I_2 \ln\left(\frac{1}{D}\right) + I_1 \ln\left(D_{1P}\right) + I_2 \ln\left(D_{2P}\right)\right) \tag{2.120}$$

Since $I_1 + I_2 = 0$, it follows that $I_2 = -I_1$, therefore [1]

$$\varphi_1 = 2 \cdot 10^{-7}\left(I_1 \ln\left(\frac{D}{r_1'}\right) + I_1 \ln\left(\frac{D_{1P}}{D_{2P}}\right)\right) \tag{2.121}$$

If point P is now moved infinitely far away then the ratio of the distance D_{1P} versus D_{2P} nears the value of 1. The ln-function of 1 is zero, therefore [1]

$$\varphi_1 = 2 \cdot 10^{-7}\left(I_1 \ln\left(\frac{D}{r_1'}\right)\right) \tag{2.122}$$

and

$$L_1 = 2 \cdot 10^{-7} \ln\left(\frac{D}{r_1'}\right) \tag{2.123}$$

This value is the same as that obtained using only the distance between the two conductors. It therefore confirms the statement that “the number of lines of flux linking conductor 1 varies from 1 before crossing the surface of conductor 2 to 0 after crossing conductor 2”. Through mathematical manipulation William D. Stevenson [1] has also shown that

$$\varphi_1 = 2 \cdot 10^{-7} \left(I_1 \ln\left(\frac{1}{r_1'}\right) + I_2 \ln\left(\frac{1}{D}\right) \right) \tag{2.124}$$

From this equation, it is clear that the total flux associated with conductor 1 is a function of the current in conductor 1 and the radius of that conductor as well as the current in the return conductor and the distance between the conductors. A similar equation can be derived for return conductor 2. The total flux and inductance obtained with this method will therefore be the same as that determined before.

2.3.7.2 Inductance of a multi-phase circuit

Using the same methods used in obtaining the total flux for a single conductor and that for a single-phase line, a set of equations was derived to determine the flux per conductor in a multi-phase circuit. The only provision yet again is for the sum of the currents in all the conductors to be equal to zero. Figure 2.28 shows a cross-sectional view of such a multi-phase circuit with reference to a distant point P [1].

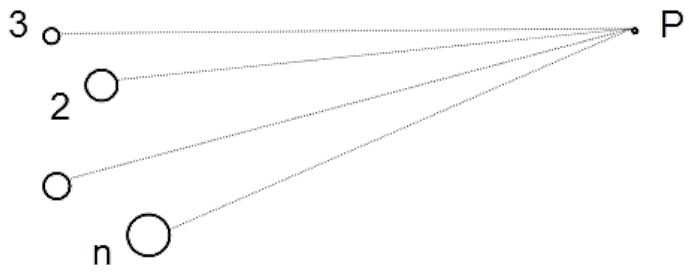

Figure 2.28: Multi-phase circuit with current vector sum equal to zero

The total flux generated in any one of these conductors is dependent on the flux generated by the current in the conductor as well as the flux generated in the conductor by the currents in the other phases. The following simplified equation, containing all the possible flux linkages of conductor 1, is obtained when point P is moved infinitely far away [1].

$$\varphi_1 = 2 \cdot 10^{-7} \left(I_1 \ln\left(\frac{1}{r_1'}\right) + I_2 \ln\left(\frac{1}{D_{12}}\right) + I_3 \ln\left(\frac{1}{D_{13}}\right) + ... + I_n \ln\left(\frac{1}{D_{1n}}\right) \right) \tag{2.125}$$

The first term in the above equation represents the self-induced flux whilst the 2nd, 3rd and other terms represents the mutually coupled flux. The same can be done for conductors 2, 3, n. D_{12}, D_{13},…D_{1n} represents the distances between conductors 1, 2, 3,….n.

$$\varphi_2 = 2 \cdot 10^{-7}\left(I_1 \ln\left(\frac{1}{D_{12}}\right) + I_2 \ln\left(\frac{1}{r_2'}\right) + I_3 \ln\left(\frac{1}{D_{23}}\right) + ... + I_n \ln\left(\frac{1}{D_{2n}}\right)\right) \quad (2.126)$$

The currents in the above equations should be represented in either instantaneous values or complex rms values.

2.3.7.3 Inductance of a single-phase composite conductor line.

A composite conductor line is a circuit where each phase consists of more than one conductor grouped together in a bundle, electrically forming a parallel circuit within the bundle. The same derivation method that was used for the single-phase two-wire line with reference to a remote point P can be used here. If we now consider a bundled conductor with all conductors within the bundle being of the same material and diameter, it follows that the current within one conductor within the bundle will be equal to the current in the bundle divided by the number of conductors within the bundle. Due to the close proximity of the different conductors within the bundle, the inductance of each of the conductors within the bundle will be affected by the alternating flux generated by the currents within each conductor of the bundle. It is interesting, although not of practical importance, since the impact is the same for all phases, to note that the current within a bundle conductor will not be shared equally by the conductors within the bundle unless transposition of conductors within the bundle is exercised.

Composite conductor circuits are essential at voltages above 230 kV, due to the corona induced power losses and the excessive interference with communication if only one conductor per phase is used [1]. For the single-phase line shown in Figure 2.29, ignoring the capacitive leakage current to earth, the sum of the current entering conductor X and that leaving conductor Y is zero. Following the same

rationale as was used for the two conductor single-phase line, equations were developed for the inductance per conductor within a bundle, the bundle itself and for the total line.

Figure 2.29: Single-phase composite conductor circuit [1]

The inductance per conductor within conductor bundle X is given by [1]

$$L_a = 2n \cdot 10^{-7} \ln \frac{\sqrt[m]{D_{aa'} D_{ab'} D_{ac'} .... D_{am}}}{\sqrt[n]{r'_a \, D_{ab} D_{ac} .... D_{an}}} \tag{2.127}$$

The variables m and n in the above equation refers to the number of conductors in conductors Y and X respectively. Due to the positioning of the conductors within a bundle, the inductance may vary between the conductors within a bundle. The average inductance (L_{av}) per conductor within a bundle is therefore given by [1]

$$L_{av} = \frac{L_a + L_b + L_c + ... + L_n}{n} \tag{2.128}$$

The total inductance per bundled conductor is then 1/n times the average inductance per bundle [1].

$$L_X = 2 \cdot 10^{-7} \ln \left[\frac{\sqrt[mn]{\left(D_{aa'} D_{ab'} D_{ac'} ... D_{am}\right)\left(D_{ba'} D_{bb'} D_{bc'} ... D_{bm}\right) ... \left(D_{na'} D_{nb'} D_{nc'} ... D_{nm}\right)}}{\sqrt[n^2]{\left(r'_a \, D_{ab} D_{ac} ... D_{an}\right)\left(r'_b \, D_{ba} D_{bc} ... D_{bn}\right) ... \left(r'_n \, D_{na} D_{nb} ... D_{nn}\right)}} \right] \tag{2.129}$$

The inductance for conductor Y is given by [1]

$$L_Y = 2 \cdot 10^{-7} \ln \left[\frac{\sqrt[nm]{\left(D_{a'a} D_{a'b} D_{a'c} \ldots D_{a'n}\right)\left(D_{b'a} D_{b'b} D_{b'c} \ldots D_{b'n}\right) \ldots \left(D_{ma} D_{mb} D_{mc} \ldots D_{mn}\right)}}{\sqrt[m^2]{\left(r'_{a'} D_{a'b'} D_{a'c'} \ldots D_{a'm}\right)\left(r'_{b'} D_{b'a'} D_{b'c'} \ldots D_{b'm}\right) \ldots \left(r'_{m} D_{ma'} D_{mb'} \ldots D_{mm}\right)}} \right] \quad (2.130)$$

where

r_a' = Geometric Mean Radius of conductor a

$D_{aa'} \ldots D_{am}$ = Distances between conductor a in composite conductor X and conductor a' through to m in composite conductor Y

$D_{a'a} \ldots D_{a'n}$ = Distance between conductor a' in composite conductor Y and conductor a through n in composite conductor X

For simplicity, the geometric mean distance and the geometric mean radius for a bundled conductor line as shown above can be replaced by D_m^X and D_s^X respectively. The superscript (x) is used to identify a specific conductor bundle associated with a phase of the circuit under consideration, whilst subscripts (m) and (s) in this case refers to mutual and self respectively.

The total inductance for this single-phase line is then given by [1]

$$L = 2 \cdot 10^{-7} \left[\ln \frac{D_m^X}{D_s^X} + \ln \frac{D_m^Y}{D_s^Y} \right] \quad (2.131)$$

It is important to note that the equation structure is essentially the same as for the simple two conductor single-phase circuit. The complex numerator and denominator replaces the distance D between the conductors and the effective radius of the conductor r' respectively. From the definition of GMD and GMR, it is therefore apparent that the numerator is the GMD between the bundle conductors of the circuit whilst the denominator is the GMR of one set of bundle conductors.

2.3.7.4 Inductance of three-phase lines with equilateral spacing

Figure 2.30 shows the conductor relationship for a three-phase line with equilateral conductor spacing of distance (D). The same conductor is used in each phase. Assuming a perfectly balanced three-phase system where the sum of the phase currents equals zero ($I_a + I_b + I_c = 0$) the following equations were developed [1]
Total flux for phase A (Self and mutually coupled flux)

$$\varphi_a = 2 \cdot 10^{-7} \left(I_a \ln \frac{1}{D_s} + I_b \ln \frac{1}{D} + I_c \ln \frac{1}{D} \right) \tag{2.132}$$

The first term reflects the self-induced flux due to the current in phase A, whilst the 2nd and 3rd terms provide the mutually induced flux caused by the currents in phases B and C respectively. Assuming a fully balanced three-phase system with equilaterally spaced conductors the current relationship $I_a = -(I_b + I_c)$ is true.

The inductance per phase for an equilaterally spaced three-phase circuit is then given by [1]

$$L_a = 2 \cdot 10^{-7} \ln \frac{D}{D_s} \tag{2.133}$$

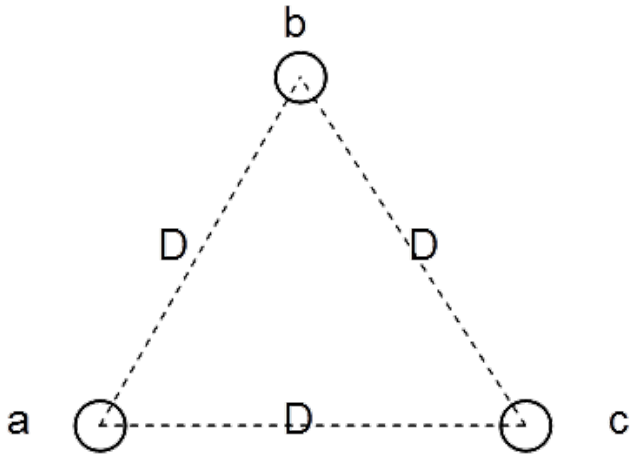

Figure 2.30: Three-phase line equilaterally spaced with no earth conductor [1]

2.3.7.5 Geometric mean diameter and radius

It is Important to note that the GMD for an equilaterally spaced circuit with uniform bundled conductors on all phases is equal to the distance between the centre points of the bundle conductors. For this situation the GMD is reflected in the equation as D only, whilst the GMR will be dependent on whether a single solid conductor or bundled conductors are used. Note that stranded conductors, also referred to as composite conductors, is also a form of bundle conductors and therefore a similar equation is used to determine its GMR [1], [18].

For three-strand bundle conductor [1]

$$D_s^b = \sqrt[n^2]{\left(D_{aa}D_{ab}D_{ac}\right)\left(D_{ba}D_{bb}D_{bc}\right)\left(D_{ca}D_{cb}D_{cc}\right)} \tag{2.134}$$

where

Daa, Dbb and Dcc = radius of conductor

Dab, Dbc; Dca = Distance between centre of conductors within bundle

n = number of conductors within the bundle

The superscript b in D^b_s refers to bundle conductor.

In an equilaterally spaced circuit with conductors of same radius, this equation can be simplified to [1]

$$D_s^b = \sqrt[3^2]{\left(D_s dd\right)^3} \tag{2.135}$$

For bolted non-ferrous metal conductor [1]

$$D_s = re^{-1/4} \tag{2.136}$$

Table 2.1 provides a summary of Geometric Mean Radius equations to be used with different conductor bundles.

Table 2.1: Geometric mean radius for bundle conductors [1]

Conductor Bundle Type	Geometric Mean Radius
Double	$D_s^b = \sqrt[4]{(D_s \cdot d)^2} = \sqrt{D_s \cdot d}$
Triple	$D_s^b = \sqrt[9]{(D_s \cdot d \cdot d)^3} = \sqrt[3]{D_s \cdot d^2}$
Quad	$D_s^b = \sqrt[16]{(D_s \cdot d \cdot d \cdot d \cdot 2^{1/2})^4} \cong 1.09 \cdot \sqrt[4]{D_s \cdot d^3}$
Hex	$D_s^b = \sqrt[36]{(D_s \cdot d \cdot d \cdot 3d^2 \cdot 2d)^6} = \sqrt[6]{D_s \cdot 6d^5}$

The basic equation to determine the GMR for stranded conductors is explained with the use of Figure 2.31 and is given by [18] to be

$$GMR = \sqrt[n_s^2]{\left(r' \cdot 2r \cdot 2\sqrt{3}r \cdot 4r \cdot 2\sqrt{3}r \cdot 2r \cdot 2r\right)^{n_s-1} \cdot r'(2r)^{n_s-1}} \tag{2.137}$$

The concept followed is the same as that for bundle conductors in that the GMR of a single strand is multiplied by the distances to all other strands that form part of the conductor. This is repeated for all strands and between all layers of the conductor. Eq. (2.137) represents the simplified equation when all the strands are of the same diameter. This equation can also be represented as shown in Eq. (2.138).

$$GMR_{sc} = \sqrt[n_s^2]{\left[D_{ss}\left(\prod_{j=2}^{n_i} d_{s_{i,j}}\right) \cdot 2r_s\right]^{n_s-1} \cdot D_{ss}(2r_s)^{n_s-1}} \tag{2.138}$$

where

D_{ss} = GMR of single strand

$d_{si,j}$ = distance between strands in same layer

r_s = strand radius

n_i = number of strands in the first layer

n_s = number of strands in conductor

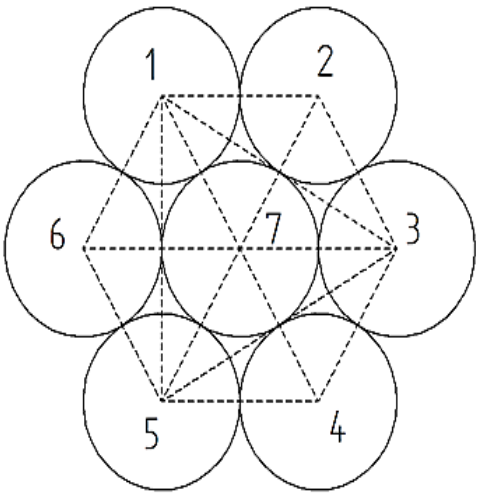

Figure 2.31: Cross-section of a stranded conductor [18]

For multi-layer stranded conductors this calculation gets rather cumbersome, and Eq. (2.137) no longer holds explicitly, since the distances between strands vary between the different layers as depicted in Figure 2.32. It therefore follows that Eq. (2.137) needs to be expanded for multi-layer stranded conductors to obtain the correct GMR for this type of conductor.

Using Figure 2.32 as reference we can clearly see that not only do the distances between the different conductor strands vary, but so also do the angular relationship between the different strands. Following the same methodology that was used by [18] to develop Eq. (2.137) we can now determine a set of equations with which to calculate the GMR for a multi-stranded ACSR conductor. In this example the steel re-enforced core is made up of 7 strands equal in size, and three aluminium layers also with the same strand size. The strand sizes are an important factor to note, since this will impact the centre distances between strands and therefore the GMR calculation.

The product of distances between strands in the first aluminium layer is then given by

$$d_{al\_L1} = \left[\prod_{k=1}^{(n_{j-1})} \sqrt{(4r_s)^2 + (4r_s)^2 - 2 \cdot (4r_s) \cdot (4r_s) \cdot \cos(k\alpha_1 \cdot \deg)} \right]^{(n_j)} \tag{2.139}$$

or

$$d_{L1} = \left(\prod_{jj} d_{a1_{ij,jj}} \right)^{(n_j)} \tag{2.140}$$

$\alpha 1$ = angle between strands on same layer with centre strand

n_j = number of strands in layer

n_{al} = number of aluminium strands in conductor

$d_{a1ij,jj}$ = distance between strands on same layer

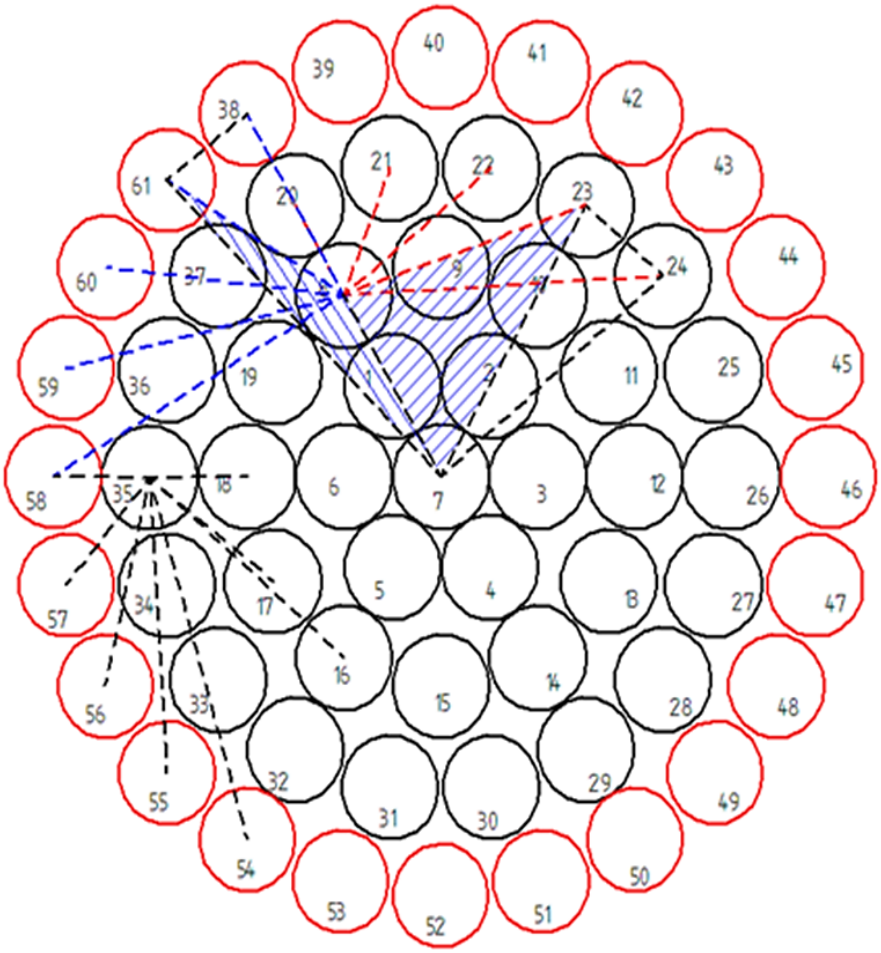

Figure 2.32: Multi-layer stranded type ACSR conductor

The distances between strands on the second layer and between layers are given by Eq. (2.141), Eq. (2.142) and Eq. (2.143)

Second Layer

$$d_{al\_L2} = \left[\prod_{k=1}^{n_k - 1} \sqrt{(6r_s)^2 + (6r_s)^2 - 2 \cdot (6r_s) \cdot (6r_s) \cdot \cos(k\alpha_2 \cdot \deg)} \right]^{(n_k)} \tag{2.141}$$

First to Second Layer

$$d_{L1\_2} = \left[\prod_{k=1}^{n_k} \sqrt{(6r_s)^2 + (4r_s)^2 - 2 \cdot (6r_s) \cdot (4r_s) \cdot \cos(k\alpha_2 \cdot \deg)} \right]^{(n_j)} \tag{2.142}$$

Second to First Layer

$$d_{L2\_1} = \left[\prod_{k=1}^{n_j} \sqrt{(6r_s)^2 + (4r_s)^2 - 2 \cdot (6r_s) \cdot (4r_s) \cdot \cos(k\alpha_2 \cdot \deg)} \right]^{(n_k)} \tag{2.143}$$

Similar equations can be created from basic mathematical principles for all other layers and combination of layers. The total geometric mean radius can then be obtained from Eq. (2.144)

$$GMR_{al} = \sqrt[n_{al}]{D_{s\_al} \cdot d_{al\_L1} \cdot d_{al\_L2} \cdot d_{al\_L3} \cdot \ldots \cdot d_{L1\_2} \cdot d_{L1\_3} \cdot d_{L2\_1} \cdot d_{L2\_3} \cdot d_{L3\_1} \cdot d_{L3\_2} \cdot \ldots} \tag{2.144}$$

Table 2.2 shows some calculation results for conductor GMR. Calculations were done using MathCAD software and are shown in Appendixes F and G. It highlights the zero impact of the inner steel core of an ASCR conductor in the calculation of conductor internal inductance due to the near zero result obtained for the steel core GMR. The calculations were slightly modified in MathCAD, as is indicated in the MathCAD example program in Appendix H, to overcome a mathematical decimal limitation that resulted in wrong answers.

Table 2.2: Example conductor GMR calculation results.

GMR Calculation result comparison (in mm)			
Conductor Type	Generic	Equation 2.144	Difference
Dinosaur	13.824	14.4336	0.6099
Earth-wire 19/2.65	$1.695 * 10^{-78}$	$533.567*10^{-9}$	$533.567*10^{-9}$

2.3.7.6 Inductance of three-phase lines with unsymmetrical spacing.

Unsymmetrical lines have different spacing relationships between the three-phases, which results in the flux linkages and therefore the inductances being different between the phases and hence an unbalanced circuit results. Different transposition techniques are used to alleviate this problem. One method is to exchange the position of the conductors such that each conductor occupies the position of every other conductor for an equal distance over the length of the line. A practice most commonly used is to change the position of conductors at switching stations in an attempt to balance the inductance of the phases across the system [1], [9].

The following equation, with the restriction that $I_a = -(I_b + I_c)$ (i.e. there is no neutral unbalance current), is used to determine the average inductance per phase for a fully transposed line [1], [9]

$$L = 2 \cdot 10^{-7} \ln\left(\frac{D_{eq}}{D_s}\right) \tag{2.145}$$

where

D_s = *Self geometric mean distance or Geometric mean radius of conductor.*

D_{eq} = *Geometric mean distance between conductors of phases a, b and c.*

The self geometric mean distance (Ds) takes into account conductor composition, stranding and bundling. Conductor composition refers to the different combinations of metal used in the construction of a conductor [2]. The calculation methods used to determine the value of Ds has already been discussed in detail in previous sections.

The geometric mean distance between conductors is given by

$$D_{eq} = \sqrt[3]{D_{ab} D_{bc} D_{ca}} \tag{2.146}$$

For non-transposed lines the total flux per phase conductor must be calculated, from which the inductance per phase can be obtained. An approximate equation for the determination of total flux for the A-phase for a non-transposed line can therefore be given as [1]

$$\varphi_a = 2 \cdot 10^{-7} \left(I_a \ln \frac{1}{D_s} + I_b \ln \frac{1}{D_{12}} + I_c \ln \frac{1}{D_{31}} \right) \tag{2.147}$$

2.3.7.7 Overhead conductor impedance matrix

The previous section and sub-sections have shown in detail the inductance calculations for different configurations of overhead lines. This section will briefly evaluate some additional factors that impact the overhead conductor impedance, their mathematical representations and finally the conductors impedance matrix. An electrical imbalance is caused by the uneven placement of high voltage overhead line conductors above earth, which results in both negative and zero-sequence currents. Standing imbalances in a high voltage system has an adverse effect in the performance of protection relays and has a heating effect in the rotors of electrical motors, generators and transformers [8].

Phase unbalance current will return via earthed earth-wires and the earth return path. J.R. Carson and others has shown that the earth return can be represented by so-called image conductors located at a distance below the earth surface equal to the respective conductor height above the earth surface [9].

The impedance matrix of a line can be subdivided into a resistance-, inductance- and suseptance matrix [11]. Attention will be given to the impedance matrix involving for now only resistance and inductance. The impedance matrix will therefore include the actual resistance (R_k) and inductive reactance (X_k) of the respective overhead

conductors, mutual resistance ($R_{k'}$) and inductive reactance ($X_{k'}$) due to each overhead conductor's image conductor [9].

The distance (D_e) in meters between the overhead conductor and its image as well as the frequency dependent resistance (r_d) of the image conductor in ohm per meter has been defined by [9], [10] and [12] as

$$D_e = 658.5\sqrt{\rho_e / f} \tag{2.148}$$

$$r_d = 9.869 \cdot 10^{-7} f \tag{2.149}$$

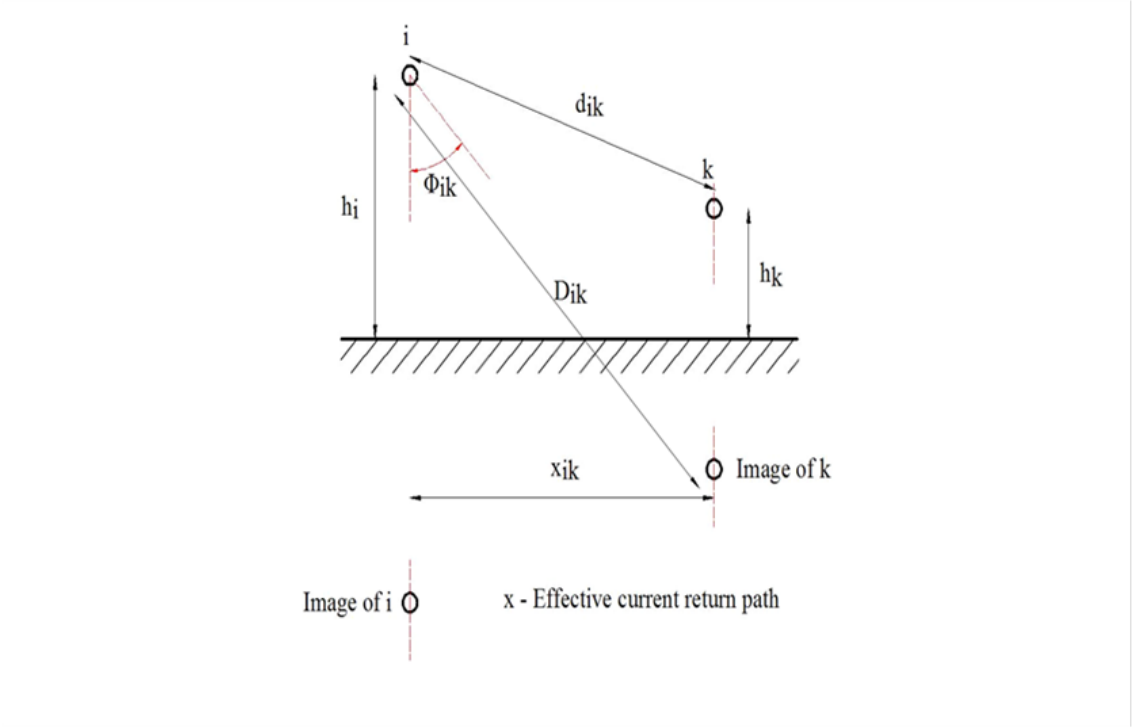

Figure 2.33: Conductor image inside earth return [11]

The values for D_e and r_d are then used in the equations for self and mutual impedance as presented by [9], [10] and [12]. The self and mutual impedance equations are shown in Eq. (2.150) and Eq. (2.151) below.

$$Z_{ii} = (r_a + r_d) + j\omega 2 \cdot 10^{-7} \ln\left(\frac{D_e}{d_{ii}}\right) \tag{2.150}$$

and

$$Z_{ik} = r_{d'} + j\omega 2 \cdot 10^{-7} \ln\left(\frac{D_{ik}}{d_{ik}}\right) \tag{2.151}$$

where

Z_{ii} = self impedance of conductor

Z_{ik} = mutual impedance of conductor

D_{ik} = distance between conductor I and image of conductor k

d_{ik} = distance between conductor I and conductor k

r_a = dc-resistance from manufacturers conductor tables

r_d = frequency dependent resistance

ρ_e = earth resistivity

A graph created in MathCAD and shown in Figure 2.34 indicates the variation of the frequency dependent resistance of the image conductor due to increase in frequency. Since the frequency dependency for resistance and depth of earth return only starts to play a significant role in the high frequencies, it will be ignored for use at 50 Hz.

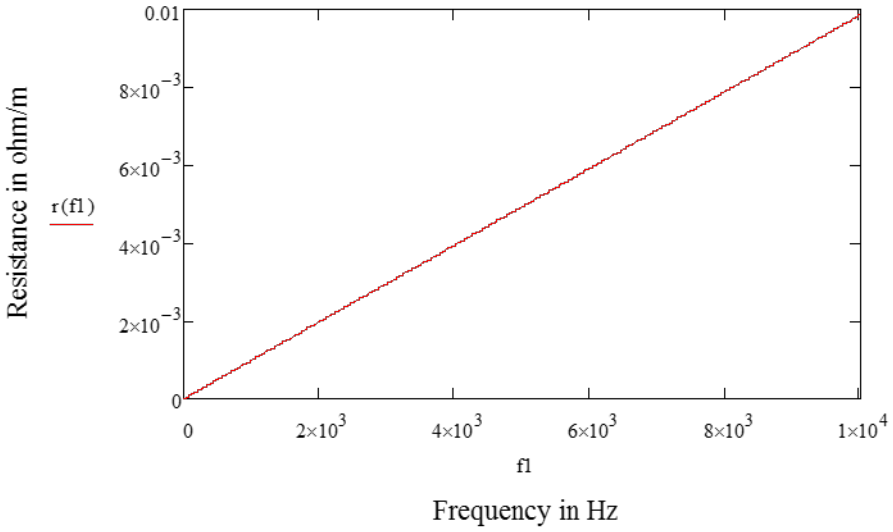

Figure 2.34: Image conductor resistance linked to frequency (Appendix G)

Equations for calculating Z_{ii} and Z_{ik} were developed by J.R. Carson and Polaczec [11] during the 1920's for telephone circuits, but are also applicable to power circuits. Gary, Deri, Tevan, Semlyen and Castanheira [11] calculate overhead line earth

return self and mutual impedances with equations proposed by Dubanton for a multi-layered earth return [11].

Earth Return Self Impedance

$$Z'_{ii} = R'_{i-\text{int}ernal} + j\left[\omega\frac{\mu_0}{2\pi}\ln\frac{2\left(h_i+\overline{p}\right)}{r_i} + X'_{i-\text{int}ernal}\right] \tag{2.152}$$

Earth Return Mutual Impedance

$$Z'_{ik} = j\omega\frac{\mu_0}{2\pi}\ln\frac{\sqrt{\left(h_i+h_k+2\overline{p}\right)^2+x_{ik}^2}}{d_{ik}} \tag{2.153}$$

with

$$\overline{p} = \sqrt{\frac{\rho_e}{j\omega\mu_0}} \tag{2.154}$$

where

$\overline{p}$ = *complex depth*

x_{ik} = *horizontal distance between conductors i and k*

ρ_e = *earth resistivity*

J.R. Carson's equations [11] considers the earth return to be a homogeneous return path while those of Hartenstein, Koglin and Rees [11] represents the earth return as multiple layers assuming uniform current distribution in each layer and having the advantage that different resistivity's can be assigned to each layer. Their method is however not a practical one, since the earth resistivity information for a multiple layer earth return is not available. Earth resistivity variations across the country make it highly possible that the earth resistivity for long lines can vary significantly over the length of the line. For practical reasons the value of earth resistivity used is standardized for use across the network. For the Eskom transmission system a resistivity value of 700 Ωm was chosen based on information that was previously obtained from tests that was performed across the country.

According to [8], [11] J.R. Carson's equation is based on the following assumptions

- The conductors are perfectly horizontal above earth, and are long enough so that three-dimensional end effects can be neglected (this makes the field problem two-dimensional).
- The sag is taken into account indirectly using an average height above earth.
- The aerial space is homogeneous without loss, with permeability ($\mu_{0)}$ and permittivity (ε_0).
- The earth is homogeneous with uniform resistivity ($\rho_{e)}$, permeability (μ_0) and permittivity (ε_0), and is bounded by a flat plane with infinite extent, to which the conductors are parallel. The earth behaves as a conductor, i.e., $1/\rho >> \omega\varepsilon_0$, and hence the displacement currents may be neglected. Above the critical frequency $f_{critical} = 1/(2\pi\varepsilon_0\rho)$, other equations must be used.
- Spacing between conductors is at least one order of magnitude larger than the radius of the conductors, so that proximity effects (current distribution within one conductor influenced by current in an adjacent conductor) can be ignored.
- The conductor profile between towers can be described
  - As a parabola for spans $\leq$ 500 m,
  - As a catenary for 500 m $\leq$ span $\leq$ 2000 m, and
  - As an elastic line for spans > 2000 m.

The average conductor height above earth is dependent on the accuracy of the parabola made by the conductor above earth and is given by the equation [11]

$$h_i = height \quad at \quad midspan + \frac{1}{3} sag \tag{2.155}$$

J.R. Carson's equation for Self Impedance, that includes the variables $\Delta R'_{ii}$ and $\Delta X'_{ii}$ for Earth Return as documented by [11] is given by

$$Z'_{ii} = \left(R'_{i-\text{int}ernal} + \Delta R'_{ii}\right) + j\left(\omega \frac{\mu_0}{2\pi} \ln \frac{2h_i}{r_i} + X'_{i-\text{int}ernal} + \Delta X'_{ii}\right) \tag{2.156}$$

and with suffixes altered to fit in with this paper, is represented by [8] as

$$Z_{ii} = R_i + 4\pi f \cdot 10^{-7}\left[j\ln\left(\frac{D_{ii'}}{GMR_i}\right) + 2(P + jQ)\right] \tag{2.157}$$

It is possible to show from basic principles that Eq. (2.156) is similar to Eq. (2.157) with the exception of the internal reactance, which has been omitted in Eq. (2.157) as well as the use of the conductor radius in Eq. (2.156), whilst the conductor GMR is used in Eq. (2.157). J.R. Carson's Earth Return Mutual Impedance as documented by [11] is given by

$$Z'_{ik} = Z'_{ki} = \Delta R'_{ik} + j\left(\omega\frac{\mu_0}{2\pi}\ln\frac{D_{ik}}{d_{ik}} + \Delta X'_{ik}\right), \text{ i} \neq \text{k} \tag{2.158}$$

where

d_{ik} = distance between conductors i and k,

D_{ik} = distance between conductor i and image of conductor k,

GMR_i = Geometric Mean Radius of conductor i

h_i = average height above earth of conductor i,

P, Q = correction terms for earth return defined by [8]*.*

r_i = radius of conductor i,

$R'_{i\text{-internal}}$ = ac-resistance of conductor i in ohm per unit length,

$X'_{i\text{-internal}}$ = internal reactance of conductor i,

$\omega = 2\pi f$, with f = frequency in Hz,

$\Delta R'$, $\Delta X'$ = J.R. Carson's correction terms for earth return effects,

and with suffixes altered to fit in with this paper, is represented by [8] as

$$Z_{ik} = 4\pi f \cdot 10^{-7}\left(j\ln\left(\frac{D_{ik}}{d_{ik}}\right) + 2(P + jQ)\right), \text{ i} \neq \text{k} \tag{2.159}$$

J.R. Carson's correction terms as obtained from [8] and [11] and used in the equation above account for the earth return effect, and are functions of the angle ϕ (ϕ = 0 for self-impedance, $\phi = \phi_{ik}$ for mutual impedance), and of the parameter (a) used in J.R. Carson's single series expansion (in SI):

$$a = 4\pi\sqrt{5}\cdot 10^{-4}\cdot D\cdot\sqrt{\frac{f}{\rho}} \tag{2.160}$$

Earth correction terms Eq. (2.161) and Eq. (2.162) shown below were obtained from [11,], whilst Eq. (2.163) and Eq. (2.164) for the same earth corrections terms, as originally defined by J.R. Carson, were obtained from [8] and [19]. The value of the constant (k) defined in Eq. (2.163) and Eq. (2.164) is given to be the same as for (a) in the calculation of the mutual impedances. A subtle difference is shown by [8] for the value of (k) in the determination of the earth correction factors (P) and (Q) for the self impedances in that the frequency is then multiplied by the earth's resistivity in Eq. (2.160). Calculations done using this variation provided a negative value for (P) and were dismissed as a typing error.

$$\Delta R' = 4\omega\cdot 10^{-7}\begin{bmatrix} \pi/8 - b_1 a\cdot\cos\phi + b_2\left((c_2-\ln a)a^2\cos 2\phi + a^2\sin 2\phi\right) \\ + b_3 a^3\cos 3\phi - d_4 a^4\cos 4\phi - b_5 a^5\cos 5\phi \\ + b_6\left((c_6-\ln a)a^6\cos 6\phi + \phi\sin 6\phi\right) \\ + b_7 a^7\cos 7\phi - d_8 a^8\cos 8\phi - .... \end{bmatrix} \tag{2.161}$$

$$\Delta X' = 4\omega\cdot 10^{-7}\begin{pmatrix} 0.5\left(0.6159315-\ln a\right) + b_1 a\cos\phi - d_2 a^2\cos 2\phi + b_3 a^3\cos 3\phi \\ - b_4\left((c_4-\ln a)a^4\cos 4\phi + \phi a^4\sin 4\phi\right) + b_5 a^5\cos 5\phi \\ + d_6 a^6\cos 6\phi + b_7 a^7\cos 7\phi \\ - b_8\left((c_8-\ln a)a^8\cos 8\phi + \phi a^8\sin 8\phi + ...\right) \end{pmatrix} \tag{2.162}$$

$$P = \begin{bmatrix} \frac{\pi}{8} - \frac{1}{3\sqrt{2}}k\cos\phi + \frac{k^2}{16}\cos 2\phi\left(0.6728+\ln\frac{2}{k}\right) + \frac{k^2}{16}\cos 2\phi\left(0.6728+\ln\frac{2}{k}\right) \\ + \frac{k^2}{16}\phi\sin 2\phi + \frac{k^3\cos 3\phi}{45\sqrt{2}} - \frac{\pi k^4\cos 4\phi}{1536} \end{bmatrix} \tag{2.163}$$

$$Q = \begin{bmatrix} -0.0386 + \frac{1}{2}\ln\frac{2}{k} + \frac{1}{3\sqrt{2}}k\cos\phi - \frac{\pi k^2}{64}\cos 2\phi + \frac{k^3\cos 3\phi}{45\sqrt{2}} - \frac{k^4\phi}{384}\sin 4\phi \\ -\frac{k^4\cos 4\phi}{384}\left(\ln\frac{2}{k} + 1.0895\right) \end{bmatrix} \tag{2.164}$$

The self and mutual impedances have also been shown by [19] to be

Self-impedance

$$Z_{ii} = Z_{Lii} + Z_{Gii} + Z_{Eii} \tag{2.165}$$

Internal Impedance

$$Z_{ii} = R_{dc} + j\omega L_{ii} \tag{2.166}$$

Mutual Impedance

$$Z_{ik} = Z_{Gik} + Z_{Eik} \tag{2.167}$$

Geometric Terms

$$Z_{Gii} = j\omega\frac{\mu_0}{2\pi}\ln\left(\frac{2h_i}{r_i}\right) \tag{2.168}$$

and

$$Z_{Gik} = j\omega\frac{\mu_0}{2\pi}\ln\left(\frac{D_{ik}}{d_{ik}}\right) \tag{2.169}$$

Earth Correction Term

$$Z_{Eii} = Z_{Eik} = \omega\frac{\mu_0}{\pi}(P + jQ) \tag{2.170}$$

where

h_i = height of conductor above earth

$j\omega L_{ii}$ = inductive reactance of conductor

$k = 2.81 * 10^{-3} * D_{ik} * (f/\rho_e)^{0.5}$

R_{dc} = dc-resistance of conductor

r_i = radius of conductor

Z_{ii} = self-impedance of conductor

Z_{Lii} = conductor internal impedance

Z_{Gii} = geometric term

Z_{Eii} = earth contribution

Table 2.4 highlights the differences in the calculated self impedance, using different methods, for a stranded ACSR A-phase conductor and a stranded 19 core earth-wire with geometric positioning as tabled in Table 2.3.

Table 2.3: Overhead Line Conductor Positioning Example

Conductor positioning (in m)		
	Horizontal	**Vertical**
A-phase	- 9.4	21.03
B-phase	0	20.724
C-phase	9.4	21.03
Earth-wire 1	- 8.3	25.15
Earth-wire 2	8.3	25.15

Table 2.4: Self Impedance Calculation Comparison

Self Impedance Calculation Results (in Ω)			
Cond. Type	J.R. Carson	EPRI – Red Book	Complex Image (J.R. Carson)
	$X_{ii} + 2\pi f \cdot \left(\frac{\mu_0}{2\pi}\right) \cdot \ln\left(\frac{2h_i}{r_i}\right)$	$2\pi f \cdot \left(\frac{\mu_0}{2\pi}\right) \cdot \ln\left(\frac{D_{ii}}{r'_i}\right)$	$\frac{j\omega\mu_0}{2\pi} \cdot \ln\left(\frac{2(p+h_i)}{r_i}\right)$
Dinosaur	j0.474989	j0.473334	0.048903 + j0.764252

Total Self Impedance Result – Inclusive of Rac and Earth Return			
Dinosaur	0.099977 + j0.759549	0.099977 + j0.757894	0.10011 + j0.76425
Earth-wire 19/2.65	1.99525 + j11.74425	1.99525 + j11.74425	1.99543 + j11.74890

Whilst the equations for the self impedance as given in Table 2.4 differ significantly, it can be shown through mathematical manipulation that the equation for J.R. Carson [11] and that obtained from the EPRI – Red Book [8], is one and the same for cylindrical conductors. The Complex Image equation differs in that it includes an approximated earth return component. When the actual GMR for a stranded aluminium steel reinforced (ACSR) conductor as used in the EPRI formula is replaced by the equivalent GMR for a solid conductor ($r.e^{-(1/4)}$), the same result ($X = j0.474989$) as that calculated by J.R. Carson is obtained for the Dinosaur conductor. Direct comparison of these equations is therefore only possible with reference to true bolted cylindrical type conductors.

The self impedance calculation results shown for the Complex Image equation differs for the Dinosaur conductor due to the use of an approximated earth correction factor, shown in the equation as (p). A close comparison is obtained when the ac-resistance and earth return factors are added to the Taylor and EPRI calculations (see Appendix G). The difference that still exists is attributed to the approximated earth return used in the Complex Image method. As already indicated previously the internal permeability of steel is equal to $875 * 10^{-6}$, whereas that for aluminium is approximately equal to that of air ($4\pi * 10^{-7}$ Hm^{-1}). No further attention will be given to this aspect, since it falls outside the intended scope of the research.

The next step prior to obtaining the impedance matrix is to evaluate the voltage drop equation for the transmission line given in Figure 2.35.

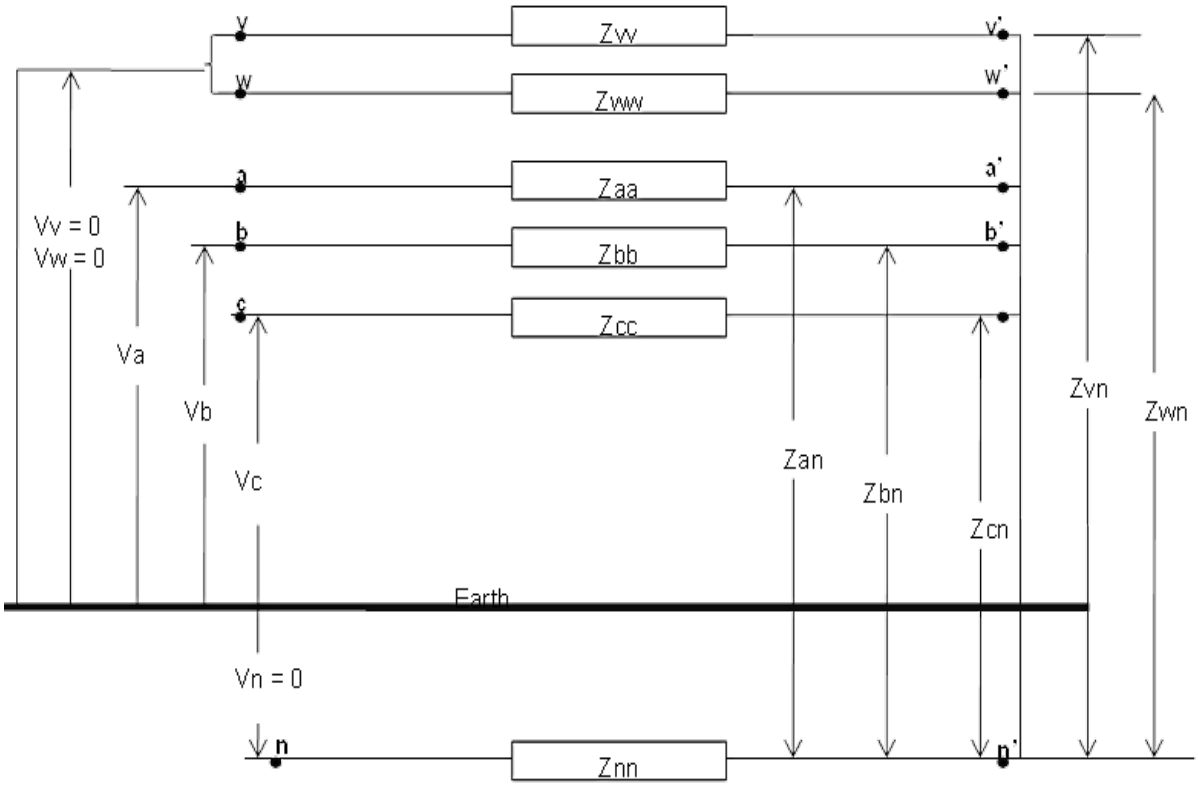

Figure 2.35: Three-phase overhead line with earth returns [9]

The voltage drop equation in per unit length in the direction of current flow can be written as follows [9]

$$\begin{bmatrix} V_a \\ V_b \\ V_c \\ V_n \end{bmatrix} = \begin{bmatrix} V_a - V_{a'} \\ V_b - V_{b'} \\ V_c - V_{c'} \\ V_n - V_{n'} \end{bmatrix} = \begin{bmatrix} Z_{aa} & Z_{ab} & Z_{ac} & Z_{av} & Z_{aw} & Z_{an} \\ Z_{ab} & Z_{bb} & Z_{bc} & Z_{bv} & Z_{bw} & Z_{bn} \\ Z_{ac} & Z_{cb} & Z_{cc} & Z_{cv} & Z_{cw} & Z_{cn} \\ Z_{av} & Z_{vb} & Z_{vc} & Z_{vv} & Z_{vw} & Z_{vn} \\ Z_{aw} & Z_{wb} & Z_{wc} & Z_{wv} & Z_{ww} & Z_{wn} \\ Z_{an} & Z_{nb} & Z_{nc} & Z_{nv} & Z_{nw} & Z_{nn} \end{bmatrix} \cdot \begin{bmatrix} I_a \\ I_b \\ I_c \\ I_v \\ I_w \\ I_n \end{bmatrix} \tag{2.171}$$

In order to reduce this matrix to a 3 X 3 matrix, we partition the matrix as shown in Eq. (2.172) [9].

$$\begin{bmatrix} E_p \\ 0 \end{bmatrix} = \begin{bmatrix} Z_A & Z_B \\ Z_C & Z_D \end{bmatrix} \cdot \begin{bmatrix} I_P \\ I_n \end{bmatrix} \tag{2.172}$$

From which we obtain two equations [9]

$$E_P = I_P Z_A + I_n Z_B \tag{2.173}$$

$$0 = I_P Z_C + I_n Z_D \tag{2.174}$$

Through manipulation of Eq. (2.173) and Eq. (2.174) we obtain Eq. (2.175) and Eq. (2.176) [9].

$$E_p = \left[Z_A - Z_B Z_D^{-1} Z_C\right] I_P \tag{2.175}$$

and

$$E_P = Z_P I_P \tag{2.176}$$

In equation Eq. (2.176) E_p represents the phase voltages, Z_p the phase impedances and I_p the phase currents. The impedance matrix of a transmission line, due to its geometrical conductor relationship, is not normally symmetrical. (i.e. the diagonal elements are equal and off-diagonal elements are equal.) The unsymmetrical 3 X 3 impedance matrix for a non-transposed transmission line can now be presented as [9]

$$Z_p = \begin{bmatrix} Z_{aaeq} & Z_{abeq} & Z_{aceq} \\ Z_{abeq} & Z_{bbeq} & Z_{bceq} \\ Z_{aceq} & Z_{bceq} & Z_{cceq} \end{bmatrix} \tag{2.177}$$

Should the transmission line be fully transposed, the elements of the impedance matrix in Eq. (2.177) are averaged, thus providing a symmetrical impedance matrix. The averaged symmetrical series impedance matrix Z_p is then [9]

$$\widehat{Z}_p = \begin{bmatrix} \widehat{Z}_{aaeq} & \widehat{Z}_{abeq} & \widehat{Z}_{abeq} \\ \widehat{Z}_{abeq} & \widehat{Z}_{aaeq} & \widehat{Z}_{abeq} \\ \widehat{Z}_{abeq} & \widehat{Z}_{abeq} & \widehat{Z}_{aaeq} \end{bmatrix} \tag{2.178}$$

where

$$\widehat{Z}_{aaeq} = \frac{1}{3}\left(Z_{aaeq} + Z_{bbeq} + Z_{cceq}\right) \tag{2.179}$$

and

$$\widehat{Z}_{abeq} = \frac{1}{3}\left(Z_{abeq} + Z_{aceq} + Z_{bceq}\right) \tag{2.180}$$

The sequence impedance matrix can now be obtained through multiplication of the averaged symmetrical series impedance matrix with A and A^{-1}, a 3 X 3 transformation matrix. The components of the matrix are obtained from the phase equations for the three-phases A, B and C when expressed in terms of their relevant sequence components. The transformation matrix A and its inverse A^{-1} is shown below in Eq. (2.181) and Eq. (2.182) [9].

$$A = \begin{bmatrix} 1 & 1 & 1 \\ 1 & a^2 & a \\ 1 & a & a^2 \end{bmatrix} \tag{2.181}$$

$$A^{-1} = \frac{1}{3}\begin{bmatrix} 1 & 1 & 1 \\ 1 & a & a^2 \\ 1 & a^2 & a \end{bmatrix} \tag{2.182}$$

The sequence matrix for the non-transposed line can now be obtained through multiplication with the transformation matrix and its inverse, shown in Eq. (2.183) [9].

$$Z_s = A^{-1} Z_p A \tag{2.183}$$

The sequence impedance matrix for the non-transposed line is therefore obtained and is shown in Eq. (2.184) below.

$$Z_s = \begin{bmatrix} Z_{00} & Z_{01} & Z_{02} \\ Z_{10} & Z_{11} & Z_{12} \\ Z_{20} & Z_{21} & Z_{22} \end{bmatrix} \tag{2.184}$$

For a fully transposed line the sequence impedances will be represented by Eq. (2.185). The outcome of which will result in a perfect diagonal matrix (e.g. all off-diagonal elements are equal to zero).

$$\hat{Z}_s = A^{-1}\hat{Z}_p A \tag{2.185}$$

The reader should by now have a good feel for what it takes to calculate the correct line series- and sequence impedance parameters. It should be clear at this point that mistakes in these calculations could have a serious impact on relay response in the system, in that significant underreach or overreach of the impedance zone elements could occur. For an example calculation of overhead line impedance, using a hypothetical configuration see Appendix G on the attached CD.

Table 2.5 shows the positive and zero sequence results obtained with the calculation methods shown above (see Appendix G and P for results shown in Table 2.5). A comparative set of results obtained from Matlab system parameter calculation software is also shown. These initial results were found to differ significantly. It was subsequently found that the relative permeability of the Dinosaur conductor is set in the database to a value of 0.8463 and the permeability of the earth-wire set to 0.9977. This is contrary to the information available from literature, which indicates that aluminium conductors should have a relative permeability close or even equal to 1.0, whilst that for steel earth-wires are approximately 700. The impact of the difference in the earth-wire permeability is significant in that for a small permeability value an inductance value comparable to that of the phase conductor is obtained. Utilising the correct permeability value for a steel earth-wire an inductance value of several hundred times bigger is obtained (see Appendix H). A relatively small difference in the conductors resistances were also found and corrected. PowerFactory had the Dinosaur and earth-wire conductor resistances set to 0.0437 Ω/km and 1.88 Ω/km, whilst MathCAD and Matlab were set to use 0.0478 Ω/km and 1.9085 Ω/km respectively.

Although the reason for this deviation between the results falls outside the immediate scope of this work, the results obtained and the default values in the conductor

database of PowerFactory were a concern. It was found that within the PowerFactory software, build version 14.1.1, the maximum value that could be set for the relative permeability of the steel earth-wire was 413 (see Appendix R). A relative permeability value of 696.3 is needed to satisfy the criteria for steel as was used in the MathCAD and Matlab calculations. Remember that the relative permeability of a specific material is given by the ratio of the absolute permeability of the material divided by the permeability of air. The absolute permeability of steel was used as 875 * 10^{-6} $H.m^{-1}$ in the calculations. Utilising a value of relative permeability in PowerFactory for the steel earth-wire of μ_r = 415 and the Dinosaur conductor μ_r = 1, the conductor parameters were re-calculated with resistances set to 0.0478 Ω/km and 1.9085 Ω/km respectively.

The results based on the changed conductor values between MathCAD and PowerFactory are shown in Table 2.6. A closer relationship was obtained for the resistances and reactances, with the exception of the zero sequence resistance. PowerFactory obtained a 26.97% larger zero sequence resistance value than the MathCAD calculation, whilst for the zero sequence reactance a 1.1% difference was obtained. Further investigation into the reasons for this was not done since it falls outside the scope of this research. It is thought however that some careful consideration should be given to this in the future as this could possibly lead to operation of protection relays for faults it was never intended to detect. Appendix Q contains the original PowerFactory result documents shown in Table 2.6. For these calculations a 275 kV tower type 517A with single Dinosaur phase conductor (template at 50° C) and dual earth-wires of type 19/2.65 (19 strands of 2.65 mm in diameter) was used.

Table 2.5: Sequence Impedance Results (MathCAD versus Matlab)

Sequence Component	MathCAD Calculation (Ω)	Matlab Calculation (Ω)	PowerFactory Calculation (Ω)
Positive Sequence	0.051221+j0.424157	0.0489+j0.564921	0.04502+j0.42095
Zero Sequence	0.190841+j1.371807	0.2612 + j1.25249	0.41943+ j1.19469

Table 2.6: Sequence Impedance Results (Matlab versus PowerFactory)

Sequence Component	MathCAD Calculation (Ω)	PowerFactory Calculation (Ω)
Positive Sequence	0.051149+j0.415683	0.0494476 + j0.423285
Zero Sequence	0.195864+j1.355747	0.2490467 + j1.323168

2.4 Load impedance and sequence networks

For most cases the impact of load and load impedances in networks during fault conditions are simply ignored. It could however, depending on the type of load and the position of a fault in the network, contribute to the overall fault current at the point of fault. A short summary of load phase and sequence impedances will be discussed in order to familiarize the user with the impact that load impedance could have during system faults.

For the purpose of this study focus will be given to balanced non-rotating loads only. The difference between rotating and non-rotating loads is non-equal positive and negative sequence impedances [9]. It is obvious that should an unbalanced three-phase load be connected to a balanced three-phase supply, unbalanced load-flow will result. Balanced loads can be connected in star, star-to-earth or delta configurations [9].

2.4.1 Balanced delta loads

A balanced delta load is obtained when three separate impedances of equal impedances are connected together in a delta formation, with the three connection points then being connected to a three-phase supply and or network (see Figure 2.36).

Equivalent sequence impedances must be determined for delta loads prior to inserting values into a sequence impedance network for analysis. Since a delta connected load does not have any earth connection, the resultant star-connection will also not have a neutral-to-earth connection. A correct delta-star load impedance transformation will result in the same line current I_a, I_b and I_c flowing into the load

before and after the transformation. For the purpose of defining the new star-connected load impedance we will ignore the source impedance. The source voltage (E) is then also the applied voltage at the load terminals.

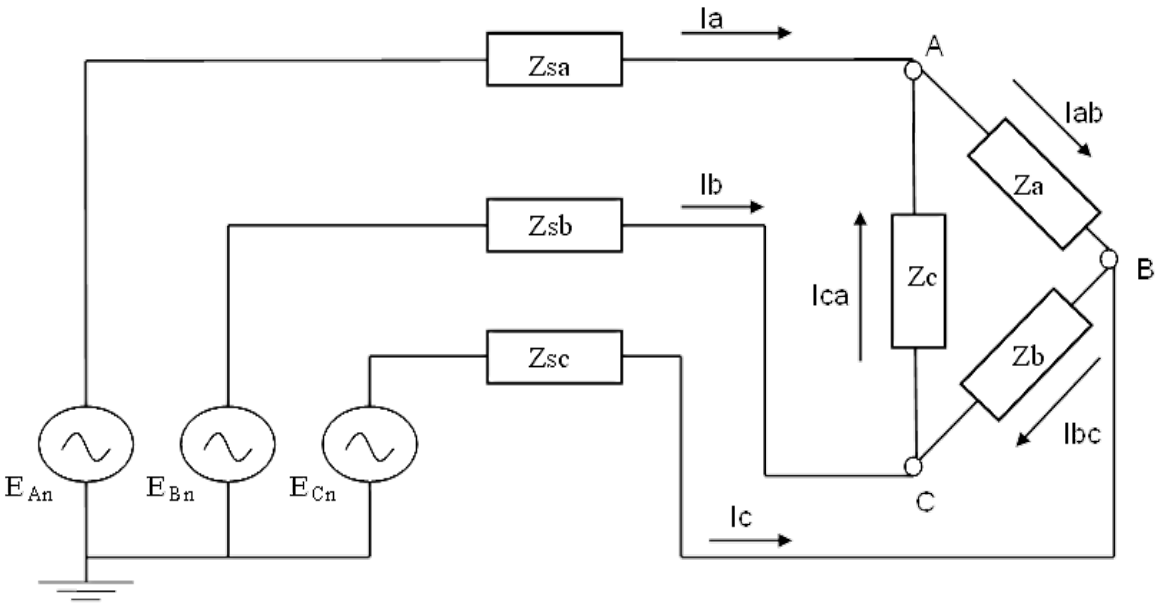

Figure 2.36: Three-phase source with Delta load

In simplification the star and delta impedances will be shown as Z_Y and Z_Δ respectively. The respective line currents for the delta and star connected loads are then given by [9]

For delta load

$$I_a = \frac{\sqrt{3}E_{ab} \cdot 1\angle -30°}{Z\Delta} \tag{2.186}$$

$$I_b = \frac{\sqrt{3}E_{bc} \cdot 1\angle -30°}{Z\Delta} \tag{2.187}$$

$$I_c = \frac{\sqrt{3}E_{ca} \cdot 1\angle -30°}{Z\Delta} \tag{2.188}$$

For star load

$$I_a = \frac{E_{ab} \cdot 1\angle -30°}{\sqrt{3}Z_{\mathrm{Y}}} \tag{2.189}$$

$$I_b = \frac{E_{bc} \cdot 1\angle -30°}{\sqrt{3}Z_{\mathrm{Y}}} \tag{2.190}$$

$$I_c = \frac{E_{ca} \cdot 1\angle -30°}{\sqrt{3}Z_{\mathrm{Y}}} \tag{2.191}$$

The equivalent star-connected impedance can now be determined using Eq. (2.186) to Eq. (2.191). Since Eq. (2.186)is equal to Eq. (2.189) we get [9]

$$\frac{\sqrt{3}E_{ab} \cdot 1\angle -30°}{Z\Delta} = \frac{E_{ab} \cdot 1\angle -30°}{\sqrt{3}Z_{\mathrm{Y}}} \tag{2.192}$$

From which we obtain the following relationship

$$Z_{\mathrm{Y}} = \frac{Z\Delta}{3} \tag{2.193}$$

The original balanced delta load can now be represented as a balanced star load, which can be analysed with the use of sequence components. This will be thoroughly discussed in the next section. Figure 2.38(b) gives an insight into the sequence circuit connections relevant to a delta/equivalent star connected load.

2.4.2 Balanced star loads

Star load configurations with star-point boltedly earthed, earthed through neutral impedance and not earthed will be covered. Figure 2.37 illustrates the phase connections of these load types to a three-phase voltage source.

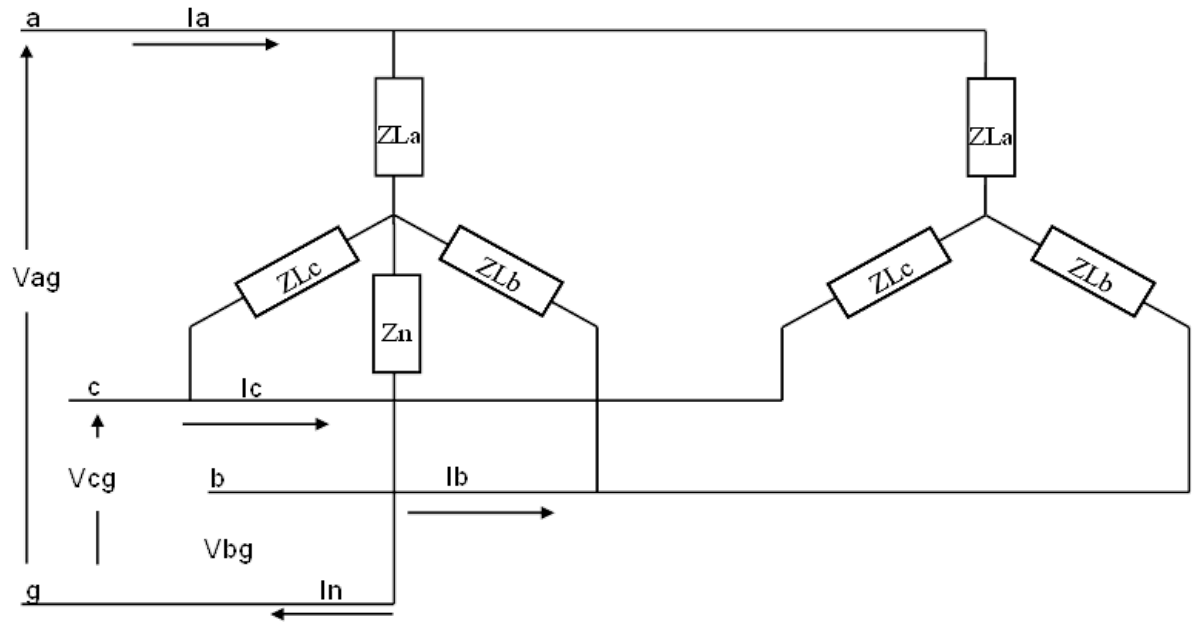

Figure 2.37: Star load configurations [9]

Phase related equations can be written for all the phase loops. The set of phase-loop equations for the earthed star-point are given in matrix format in Eq. (2.194) [9].

$$\begin{bmatrix} Vag \\ Vbg \\ Vcg \end{bmatrix} = \begin{bmatrix} (Z_Y + Z_n) & Z_n & Z_n \\ Z_n & (Z_Y + Z_n) & Z_n \\ Z_n & Z_n & (Z_Y + Z_n) \end{bmatrix} \cdot \begin{bmatrix} I_a \\ I_b \\ I_c \end{bmatrix} \tag{2.194}$$

Utilizing the simplified phase loop matrix equation, Eq. (2.176) the transformation matrix A and its inverse A^{-1} shown in Eq. (2.181) and Eq. (2.182), phase voltage matrix equation, Eq. (2.194) can be written into the sequence matrix for balanced star-connected load shown in Eq. (2.195) below [9].

$$Z_s = \frac{1}{3} \cdot \begin{bmatrix} 1 & 1 & 1 \\ 1 & a & a^2 \\ 1 & a^2 & a \end{bmatrix} \cdot \begin{bmatrix} (Z_Y + Z_n) & Z_n & Z_n \\ Z_n & (Z_Y + Z_n) & Z_n \\ Z_n & Z_n & (Z_Y + Z_n) \end{bmatrix} \cdot \begin{bmatrix} 1 & 1 & 1 \\ 1 & a^2 & a \\ 1 & a & a^2 \end{bmatrix} \tag{2.195}$$

The sequence matrix can be simplified through the normal matrix multiplication and the use of the mathematical identity $(1 + a + a^2) = 0$ for balanced load, and then written in the sequence circuit equation shown in Eq. (2.196) [9].

$$\begin{bmatrix} V_0 \\ V_1 \\ V_2 \end{bmatrix} = \begin{bmatrix} (Z_Y + 3Z_n) & 0 & 0 \\ 0 & Z_Y & 0 \\ 0 & 0 & Z_Y \end{bmatrix} \cdot \begin{bmatrix} I_0 \\ I_1 \\ I_2 \end{bmatrix} \quad (2.196)$$

Three separate sequence equations representative of the load sequence networks have been shown to be [9]

$$V_0 = I_o(Z_Y + 3Z_n) \quad (2.197)$$

$$V_1 = I_1 Z_Y \quad (2.198)$$

$$V_2 = I_2 Z_Y \quad (2.199)$$

The same set of equations could be used for unbalanced load, with the difference that the resultant matrix will however have off-diagonal values due to the differences in the load phase impedance values. It is important to note from Eq. (2.197), Eq. (2.198) and Eq. (2.199) that the positive, negative and zero-sequence load impedance would be equal when the load star-point is boltedly earthed (i.e. $3Z_n = 0$). The neutral impedance Z_n has an infinite value when the load star-point is isolated from earth. In this situation there will be no current path to earth, no zero sequence current can exist and an open-circuit condition is therefore created in the load's zero sequence circuit [9]. It must be noted that as a load is connected to the power network through a star-star transformer or an auto-transformer with the neutral points earthed, such a load will present itself to the network via the transformers as an earthed load provided that the load itself is also connected in star and earthed.

It should also be noted that a zero sequence current in the load star-point can exist in the event of an unbalanced voltage source consisting of zero sequence voltage being connected to a balanced star-earth connected load. Figure 2.38(a) represents a star-connected load with the load star-point connected to earth, either boltedly or through neutral impedance [9].

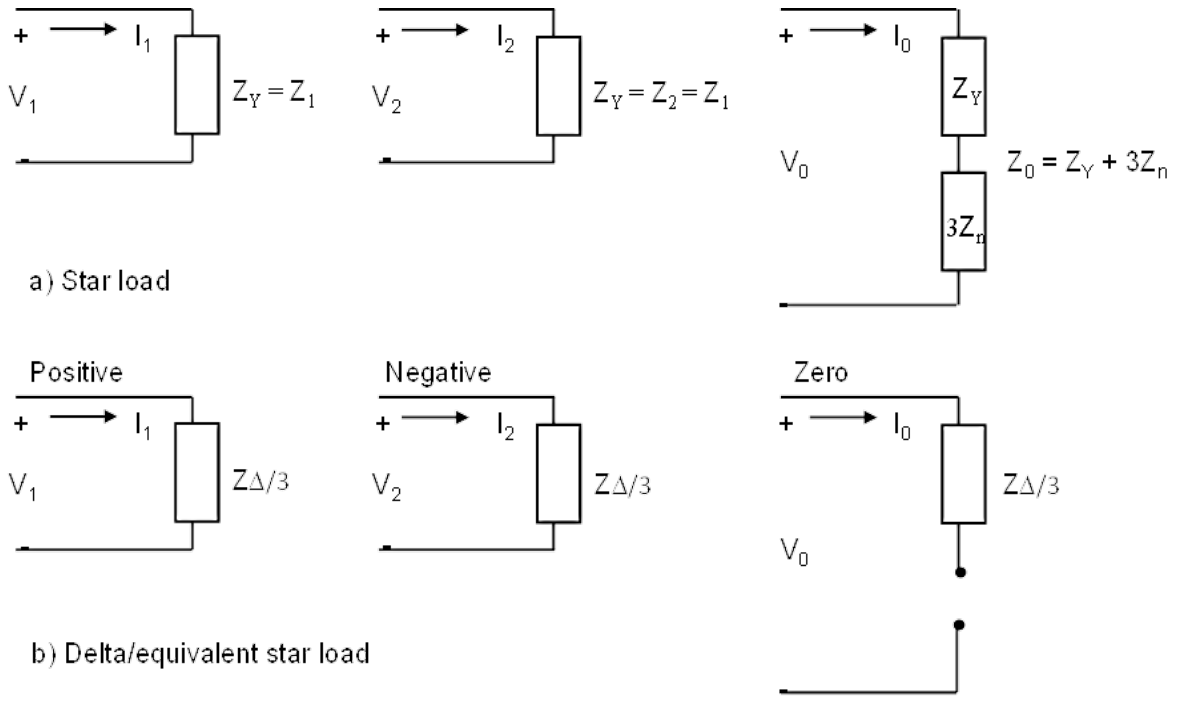

Figure 2.38: Positive, negative and zero sequence circuits for balanced load [9]

The impact of load on impedance protection on high voltage networks will be analysed in more detail in Chapter 4.

2.5 Summary

This chapter covered the basics of different earth fault loops and illustrated the complexity of overhead line impedance calculations from first principles. Differences that exist in complexity between radial and complex networks and in the sequence networks for different types of loads were also highlighted. The impact of factors such as skin effect, proximity effect, spiralling of conductor strands and transformer effect in ACSR type conductors were discussed. The inductance calculations for single-phase, multi-phase and three-phase circuits were analysed in detail. The purpose was to provide a theoretical basis for overhead line inductance calculations. Wrongly calculated overhead line inductance will have a major impact on the overall line impedance and therefore also in the calculated relay settings. This in turn could result in relay maloperation that can impact supply.

The following two chapters (Chapter 3 and Chapter 4) will attempt to highlight the measurement techniques used by different relays as well as the different elements/functions involved with two of the numerical impedance relays in use on the 400 kV transmission network in the Eskom system. The impact that line impedance, series compensation, fault resistance and load has on their relevant measurements will also be shown.